LA-UR-13-21081
Approved for public release; distribution is unlimited.

Title:	FINAL REPORT Multipurpose Acoustic Sensor for Downhole Fluid Monitoring
Author(s):	Pantea, Cristian
Intended for:	Report

FINAL REPORT

Multipurpose Acoustic Sensor for Downhole Fluid Monitoring

Project Technology Type

EGS Component R&D › High-Temperature Downhole Tools

Awardee

Los Alamos National Laboratory

Objectives

- Develop a multipurpose acoustic sensor for downhole fluid monitoring in Enhanced Geothermal Systems (EGS) reservoirs over typical ranges of pressures and temperatures and demonstrate its capabilities and performance for different EGS systems. Figure 1 shows a conceptual picture of an EGS
- Determine in real-time and in a single sensor package several parameters: temperature, pressure, fluid flow and fluid properties.
- Needed in nearly every phase of an EGS project, including Testing of Injection and Production Wells, Reservoir Validation, Inter-well Connectivity, Reservoir Scale Up and Reservoir Sustainability.
- Current sensors are limited to operating at lower temperatures, but the need is for logging at high temperatures. The present project deals with the development of a novel acoustic-based sensor that can work at temperatures up to 374°C, in inhospitable environments.

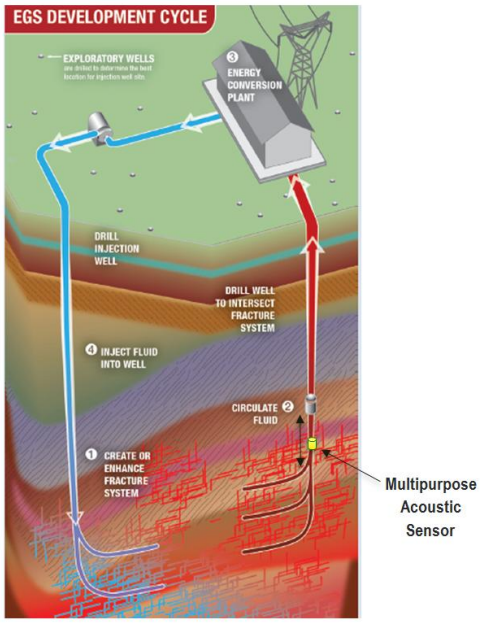

Figure 1. Illustration of EGS development cycle and Multipurpose Acoustic Sensor.

Technical Barriers and Targets

- This project addresses directly the Site/Well Characterization Barrier D: Characterization – Subsurface environments in EGS regimes are inhospitable to existing downhole, in-situ characterization methods.
- Demonstrate sensor capabilities that can be employed at a depth of 220 bar and operation temperatures of 374 °C.
- Technical targets

Task 1: Materials identification (Sep 2009 – Jun 2010)

Milestone: Identify materials that can withstand P-T conditions present in EGS systems (M1).

Task 2: Theoretical modeling and algorithm development (Jan 2010 - Jul2012)

Milestone: Develop and verify theoretical model for fluid properties determination (M2).

Decision Point: Gate 1: Identification of appropriate materials

Task 3: Sensor geometry (Jul 2010 – Apr 2012)

Milestone: Optimized sensor geometry (M3)

Decision Point: Gate 2: Identification of sensor geometry with potential to meet requirements

Task 4: Flow measurement and fluid composition (Apr 2011 – Apr 2012)

Milestone: Determine fluid composition and flow for fluids characteristic to EGS (M4)

Task 5: Temperature and pressure calibration (Jul 2011 – Apr 2012)

Milestone: Determine the relationship between pressure, temperature and transducers resonances (M5)

Overview

– Timeline
  - Project start date: Oct 2009
  - Project end date: Sep 2012
  - Percent complete: 100 %

  * Received 71% of the original allocated funds. Re-casted delivered funds to cover a 3-year period.

– Budget
  - Total project funding: $ 1,138,450

- DOE share: $ 1,138,450
- Awardee share: $ 0
- Total spent: 100% ($1,138,450)

– Barriers
  - Site/Well Characterization Barrier D: Characterization – Subsurface environments in EGS regimes are inhospitable to existing downhole, in-situ characterization methods.
  - Demonstrate sensor capabilities that can be employed at a depth of 220 Bar and operation temperatures of 374°C.

Relevance/Impact of Research

- Novel sensor design ***based on acoustics***.
- Determine in **real-time** and in a **single sensor package** multiple parameters: temperature, pressure, fluid flow; and fluid properties, such as density, viscosity, fluid composition.
- Needed especially in Site/Well Characterization.
- All components, such as transducers, cables and electronics are commercially available.
- The unique design of the sensor allows its operation at very high temperature and pressure (22 MPa and 374°C). The active parts of the sensor are piezoelectric materials that can withstand adverse conditions of very high pressure and temperature.
- Advantages: (1) low power consumption, (2) all solid-state and rugged, (3) can withstand high temperature and pressure, (4) low cost, and (5) will replace 5-7 current instruments with a single one.

Funding Opportunity Announcement

DE-PS36-09GO99017: Laboratory Call for Submission of Applications for Research, Development and Analysis of Geothermal Technologies.

Funding Source

American Recovery and Reinvestment Act of 2009

DOE Funding Level

Total Award: $1,138,450

Total Project Cost

$1,138,450

Principal Investigator(s)

Cristian Pantea

Co-Investigators

Blake T. Sturtevant

Dipen N. Sinha

Description of Technical Approach

This project proposes a truly unique and novel sensor design that is based on acoustics and can determine in real-time and in a single sensor package several parameters: temperature, pressure, fluid flow and fluid properties, like sound speed, sound absorption, etc. A versatile sensor such as this also has similar applications in several industries including the oil and gas industry, chemical industry, pharmaceutical industry and there are excellent opportunities to partner with such industries as the project progresses. The sensor can also be adapted for use in surface pipes.

Fluid composition including density and viscosity at various depths in a borehole provides geothermal reservoir properties.

Borehole temperature at various depths provide diagnostic measurements for geothermal reservoir characterization: determines thermal gradient along the borehole, provides location of borehole fracture intersections, allows estimation of thermal drawdown, and recovery rates of the circulating systems. The temperature provides diagnostic data during drilling, cementing, pressurization, and hydraulic-fracturing operations.

Borehole pressure at various depths determines pressure gradient along the borehole, provides location of borehole fracture intersections, can provide information related to recovery rates of the circulating systems.

Fluid flow determination provides fluid-flow patterns in a borehole. A typical borehole has fractures in several zones. The fluid flow can help characterize the man-made reservoir by: determining the nature and location of the fractures, determining the location and the amount of fluid that leaves and enters the borehole, and determining the relative contribution of each fracture to the total reservoir.

More than 97% of the United States' land area at depths up to 10 km are at temperatures of 250°C or lower, making this temperature an ideal target temperature for characterization instruments. In addition to high temperature challenges, the fluids in geothermal systems are chemically harsh brines which are very corrosive, particularly at high temperatures. Sound speed varies with many physical parameters of a liquid such as temperature, pressure, and dissolved solid or gas content. Thus, when used with complimentary characterization tools, sound speed provides valuable information regarding the dynamics of a fluid system. We report here on the development of an acoustic resonance cell for sound speed measurements that is capable of performing at this elevated temperature, is mechanically rugged, and offers a precision better than 0.1%. This measurement cell has been repeatedly used at temperatures up to 250°C and pressures up to 3000 psig.

The underlying physical basis of the sensing technique proposed here is Swept Frequency Acoustic Interferometry (SFAI) and resonance tracking. We propose to adapt SFAI and combine certain new approaches to extract multiple fluid parameters from a single sensor. The SFAI technique involves the determination of the frequency response of a solid container and the fluid inside it over a wide frequency range. This spectrum consists of a series of regularly spaced resonance peaks that originate from standing waves set up in the fluid-filled sensor cavity. The *sound speed* is determined from the frequency spacing between any two consecutive resonance peaks while the width of the peaks as a function of frequency is related to the *sound attenuation* in the fluid. Additionally, a more complex data analysis can provide other fluid properties, including fluid composition, viscosity, and density. For every material, there is an interdependent relationship between its fundamental resonance frequency and temperature, which can give accurate *temperature* determination.

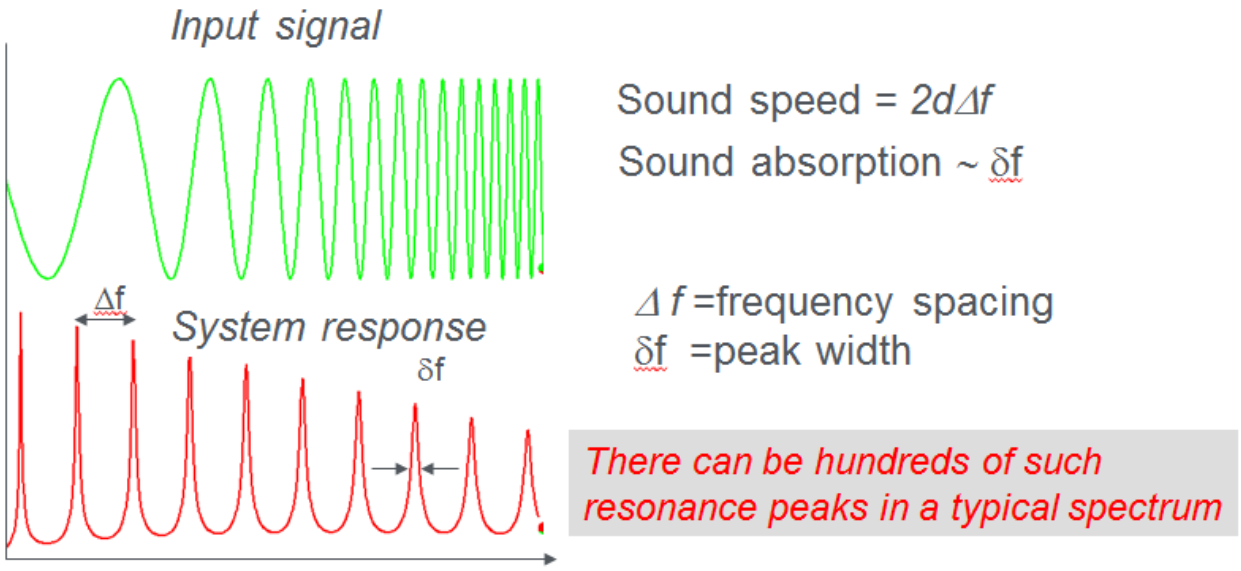

Figure 2. Illustration of the Swept Frequency Acoustic Interferometry (SFAI) technique.

A cross-correlation analysis of the frequency spectrum on a dual electrode design on the piezoelectric cylinder provides *fluid flow* measurement. Piezoelectric materials that can withstand high temperatures of 400°C or higher are commercially available and have been used by us in the past. The design of the proposed sensor has the advantage that there is no differential pressure on the sensor and thus can withstand very high pressures (22 MPa or higher) without any damage. Resonance-based methods are well-known for higher absolute accuracy and much smaller S/N ratio. See, *e.g.* Migliori A, Sarrao J. Resonant ultrasound spectroscopy. New York: Wiley-Interscience; 1997.

Important Advantages of SFAI:

- Requires very little power (~ a few mW) for high quality measurements.
- Can resolve changes in fluid (pure liquid, mixtures, suspension, emulsions, etc.,) properties to ppm levels in a continuous manner.
- Can be used for continuous tracking of fluid properties
- Very high signal-to-noise ratio (~ 92 dB) without signal averaging
- Measurement made with narrow band tracking filter.
- Allows characterization of a fluid through multiple interfering layers
- Arbitrary frequency range can be studied with any desired frequency resolution
- Absolute amplitude information is not important and so transducer quality is not an issue.
- Direct frequency domain measurement without going through pulse echo-data and Fourier transform of such data.
- Measurements can be made even with a single transducer
- Well suited to characterize emulsions & suspensions.

Figure 3 depicts the block diagram of the measurements approach. Basically, temperature and pressure determination are independent of other conditions. The sound speed, sound absorption and/or fluid composition are determined at a certain pressure and temperature. Additionally, the fluid flow is independent of temperature and pressure.

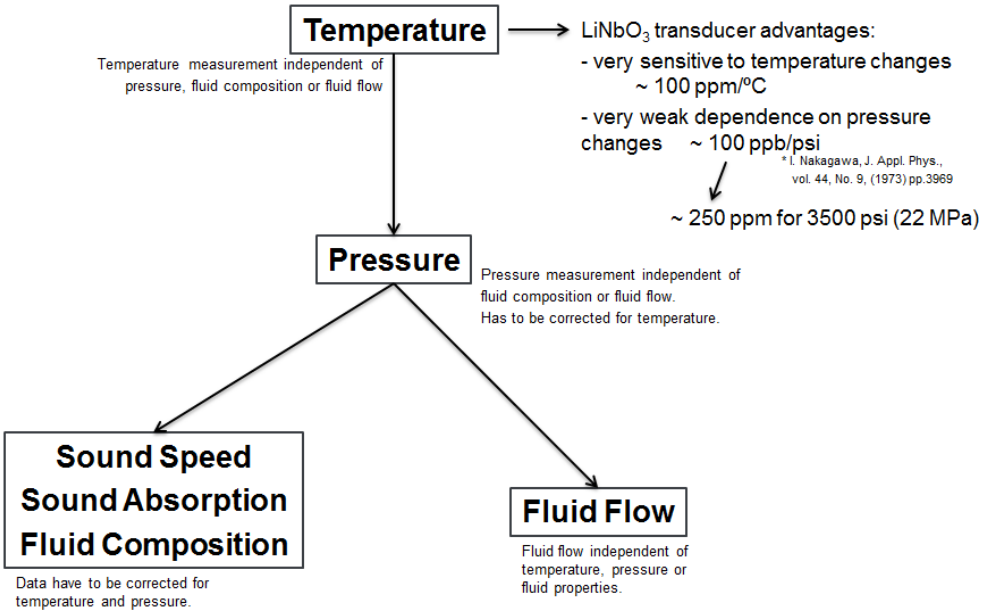

Figure 3. Chart showing the inter-dependence of parameters determined with the LANL sensor.

Project Management, Targets/Milestones

Project management tasks consisted of:

- Coordinating the work performed by the team.
- Coordinating and mentoring postdoc.
- Monthly checks on budget situation.
- Constant monitoring of work performed and future directions.
- Spending according to plan, see Figure 4. Fluctuations are due to a slow start, and later on due to major equipment acquisition.

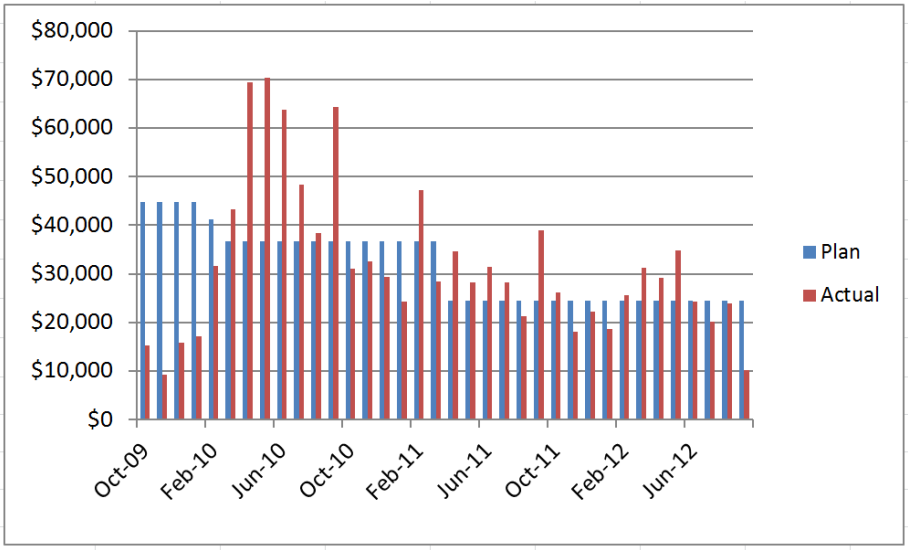

Figure 4. Spend plan

This project includes seven inter-related technical tasks, as well as an overall project management and reporting task. Specific Go/No Go decision points have been included in the development process, to ensure appropriate direction, and redirection if necessary, throughout the project. The inter-relationship of the tasks is illustrated in the Gantt chart (Figure 5), which also includes our proposed milestones and decision points.

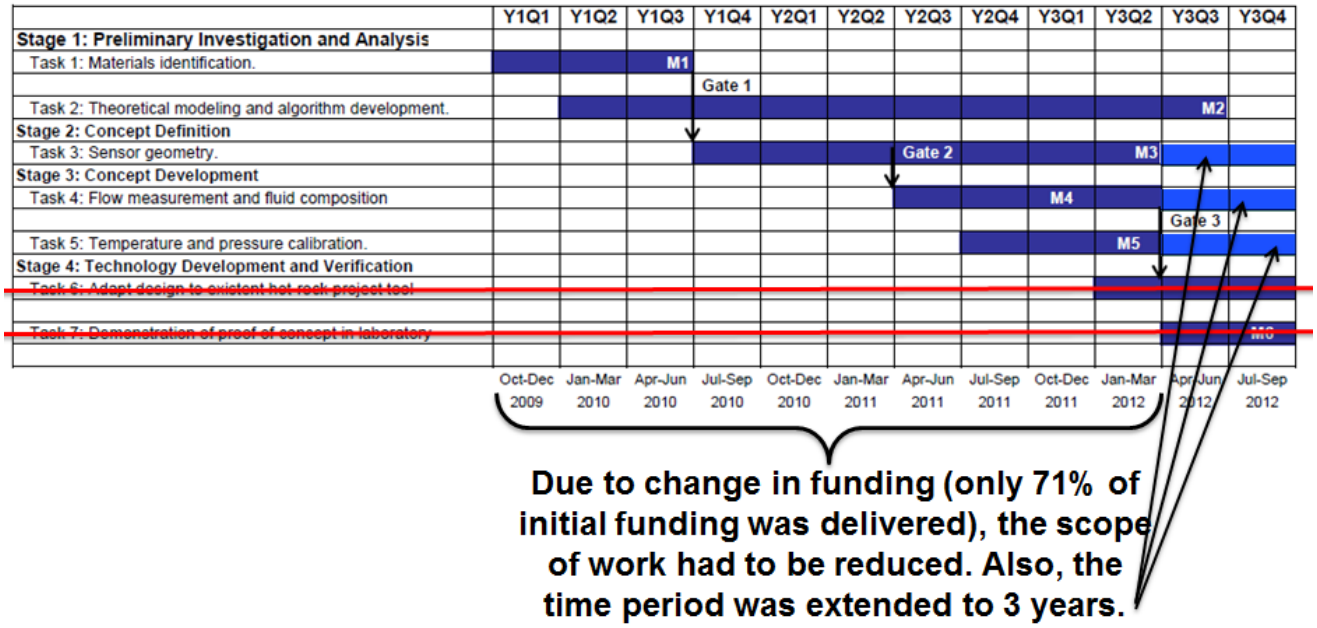

Figure 5. Gantt chart of the work proposed.

Stage 1: Preliminary Investigation and Analysis

Based on past work related to SFAI technique, the preliminary investigation and analysis of the proposed sensor requires only the identification of the right choice of materials for the sensor.

Task 1: Materials identification

Several types of *piezoelectric materials* with high Curie temperatures will be tested at high temperatures and pressures to determine their feasibility at such conditions. This is a crucial aspect of this project.

Proper choice of *electrically conductive solder and epoxy operable at high-temperature* conditions will also be investigated. Electrical connections between the acoustical sensor and the transmission cable have to survive for extended period of times in adverse conditions of temperature. *Cable insulation* is prone to temperature degradation and the right material needs to be chosen.

Milestone: Identify materials that can withstand P-T conditions present in EGS systems (M1).

Task 2: Theoretical modeling and algorithm development

Develop sensor model for efficient extraction of multiple fluid properties. To extract fluid properties in real time, efficient algorithms for data processing need to be developed. This will include specialized joint time-frequency signal processing techniques.

Milestone: Develop and verify theoretical model for fluid properties determination (M2).

Decision Point: Gate 1: Identification of appropriate materials

Stage 2: Concept Definition

Task 3: Sensor geometry

Piezoelectric materials of cylindrical, parallelepiped and other geometries will be investigated. The high-pressure characteristic to EGS systems has to be accounted for. Hard ceramic material with piezoelectric material attached on the sides will be also tested for resistance to pressure and temperature. The most efficient geometry will be tested for best accuracy in fluid properties determination.

Milestone: Optimized sensor geometry (M3)

Decision Point: Gate 2: Identification of sensor geometry with potential to meet requirements

Stage 3: Concept Development

Task 4: Flow measurement and fluid composition

Several adaptations of the SFAI technique will be investigated to determine the optimum approach for flow measurements. These will include flow-induced vibration and various cross-correlation techniques.

Investigate sensitivity and reliability of fluid composition for different material components present in a typical EGS system.

Milestone: Determine fluid composition and flow for fluids characteristic to EGS (M4)

Task 5: Temperature and pressure calibration

The piezoelectric material chosen in Task 1 has to be properly calibrated in the pressure-temperature space. Derive the equation that will link pressure and temperature on the acoustical resonances of the sensor. Investigate the sensitivity and reliability of the pressure and temperature measurements.

Milestone: Determine the relationship between pressure, temperature and transducers resonances (M5)

Decision Point: Gate 3: Laboratory prototype developed

Stage 4: Technology Development & Verification

Task 6: Adapt design to existing hot dry rock project tool in a confined geometry

Adaptation of acoustical sensor to existing high pressure-high temperature tools, and improvement (Hot Dry Rock Project at LANL, funded by DOE until 1985).

Task 7: Demonstration of proof of concept in laboratory

The proof of concept of the acoustical sensor will be demonstrated in the laboratory, in conditions similar to the one present in a typical EGS system.

Milestone: Demonstrate the proof of concept in a laboratory setup that simulates EGS conditions (M6)

*Obs: as shown in Figure 5, the Stage 4 of this project was eliminated from the scope of the project, due to change in funding: only 71% of the promised funding was delivered.

Results and Accomplishments

1. Materials Identification

1.1. High Temperature Transducers

Common transducers have low Curie Temperature (T_C). High T_C is desirable because the transducer loses its piezoelectric property as the temperatures approach T_C. The most commonly used transducers are the PZT (Lead Zirconate Titanate: $Pb[Zr_xTi_{1-x}]O_3$, $0<x<1$). However, as seen in Table 1, their Curie temperature is very low, 195-300°C, depending on the composition. Another common transducer material used often especially in temperature determinations is Quartz, which has slightly higher T_C, but can't be used for long durations in high temperature applications, especially in the higher range requested in the call for this project (374°C). Three other types of materials were investigated: Lithium Niobate, Langatate and Langasite, all with higher Curie Temperature. For long term operation, it is considered safe to use a transducer up to temperatures about half of their T_C.

We decided to work with Lithium Niobate transducers because these are available commercially in the US. The Langatate and the Langasite are also very promising but not that easy to come by, as these are newly discovered piezoelectric materials, still under investigation by the scientific community.

Table 1. Transducer Materials

Material Name	Chemical Formula	Curie Temperature T_C (°C)
PZT	$Pb[Zr_xTi_{1-x}]O_3$	195-300
Quartz	SiO_2	573
Lithium Niobate	$LiNbO_3$	1150
Langatate	$La_3Ga_{5.5}Ta_{0.5}O_{14}$	> 1200
Langasite	$La_3Ga_5SiO_{14}$	> 1200

1.2. *High Temperature Coaxial Cable*

Electrical excitation signal transmission down to the sensor and the acoustical signal detected by the sensor transmitted back up to the surface require coaxial cable that can withstand the adverse conditions of high pressure, high temperature and corrosion present in a typical EGS. In the past, we successfully used coaxial cables that could withstand high temperatures up to 350°C. For this specific case we had to perform a search for a different cable, as higher temperatures and more corrosive media are present. We selected a High Temperature – High Frequency (HTHF) Coaxial Cable that can withstand temperatures up to 600°C, and can work in very aggressive media. These cables are suitable for transmission of signals with frequencies up to 20 GHz. The signal attenuation of the cable is approximately 0.5 dB/km/MHz, and the characteristic impedance is 50 Ω.

The HTHF coaxial cable consists of a Copper core, copper lined stainless steel sheath, while the insulator is mineral powder, see Figure 6 below.

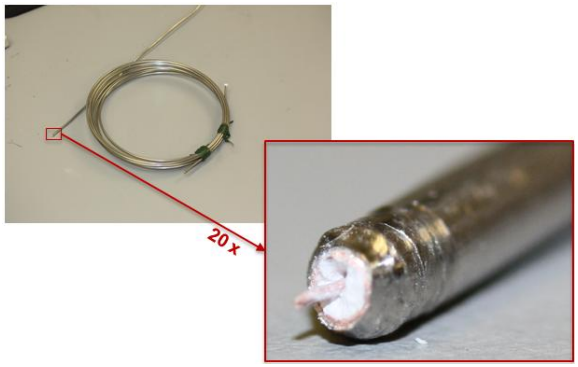

Figure 6. High Temperature - High Frequency coaxial cable.

The HTHF coaxial cables with outside diameter of 1mm and 2 mm were successfully tested, together with a Lithium Niobate transducer, at high temperatures up to about 400°C.

1.3. Pressure Vessel

To simulate the conditions of high pressure and high temperature characteristic to EGS, a Parr Instruments pressure vessel was acquired. Figure 7 shows a picture of the pressure vessel, with a working volume of 1 liter. A sufficiently large volume was chosen to be able to accommodate sensors of different geometries and sizes. The maximum pressure attainable is 41 MPa, while the maximum temperature is 600°C. These limits are much higher than the maximum pressure and temperature conditions from the call for this project (22 MPa and 374°C).

Figure 7. Parr Instruments pressure vessel.

The pressure vessel is rated to 500°C and 5000 PSI (model# 4681, Parr Instrument Company, Moline, IL) and it was used as a test environment for demonstrating the measurement cell. The 1 liter volume of the pressure vessel was filled with 700 mL of distilled, degassed water. The measurement cell itself occupies a volume of ~100 mL and the remaining ~200 mL headspace consisted of nominally whole air. The signal-carrying coaxial cables were sealed to the pressure vessel using Grafoil gland compression fittings (MHM2 series, Conax Technologies, Buffalo, NY). The pressure vessel is fitted with a furnace heater and temperature controller, see Figure 8. The internal pressure can be controlled independently of temperature by pressurizing the headspace in the vessel. Because a freshly filled gas cylinder can provide a maximum pressure of ~2300 psi, a pressure amplifier with a 30:1 piston head area ratio (Model: AAD-30, Haskel International, Inc., Burbank, CA) was used to enable repeated testing up to 3000 psi. An 80 psig house air source was used to drive the amplifier and a compressed N_2 cylinder provided the working gas at a pressure of ~1000 psig on the low pressure side of the regulator.

The temperature inside the water test fluid was monitored with an accuracy of ±1.1°C or 0.4% of the reading (whichever is greater) and a precision of ±0.1°C using a type-J thermocouple (Model M8MJSS-M2-U-250, Omega Engineering, Inc.). The system pressure was measured to an accuracy of ±13 psi using a pressure transducer with a 0-5000 psig range (Model PX309-5KG5V, Omega Engineering, Inc.). To collect the data shown below, a vector network analyzer (Model Bode 100, OMICRON electronics Corp. USA, Houston TX) was used to measure the S_{21} transmission scattering parameter.

Figure 8. High Pressure - High Temperature System, 5000 psi @ 500 C

1.4. Cable length

The electronics necessary to run the suite of sensors used in this project is situated at the top of the borehole, eliminating the need for any high-temperature electronics. It was desirable to avoid the need for such electronics, as they are still in development, and they cannot reach the high temperatures used in this project at this time.

Consequently, long coaxial cables have to be used. In order to investigate the effect of cable attenuation, we performed several experiments with different coaxial cable lengths. Attenuation is proportional to f^2, meaning that low frequency signal varies significantly less with cable length. SFAI spectra collected using between 20 and 15,020 feet of coaxial cable are shown in Figure 9. We are interested in relatively low frequencies, up to about 5 MHz, but we used a relatively large frequency range, up to 30 MHz.

Attenuation data versus cable length, for the resonance at 840 kHz, are shown in Figure 10. At the longest cable length used, the attenuation was about two orders of magnitude higher than for the shortest cable length used. However, because we are working in the frequency-domain, more precisely,

we are determining small changes in frequency, the signal still has a magnitude that can be used easily for the data analysis needed in the SFAI technique.

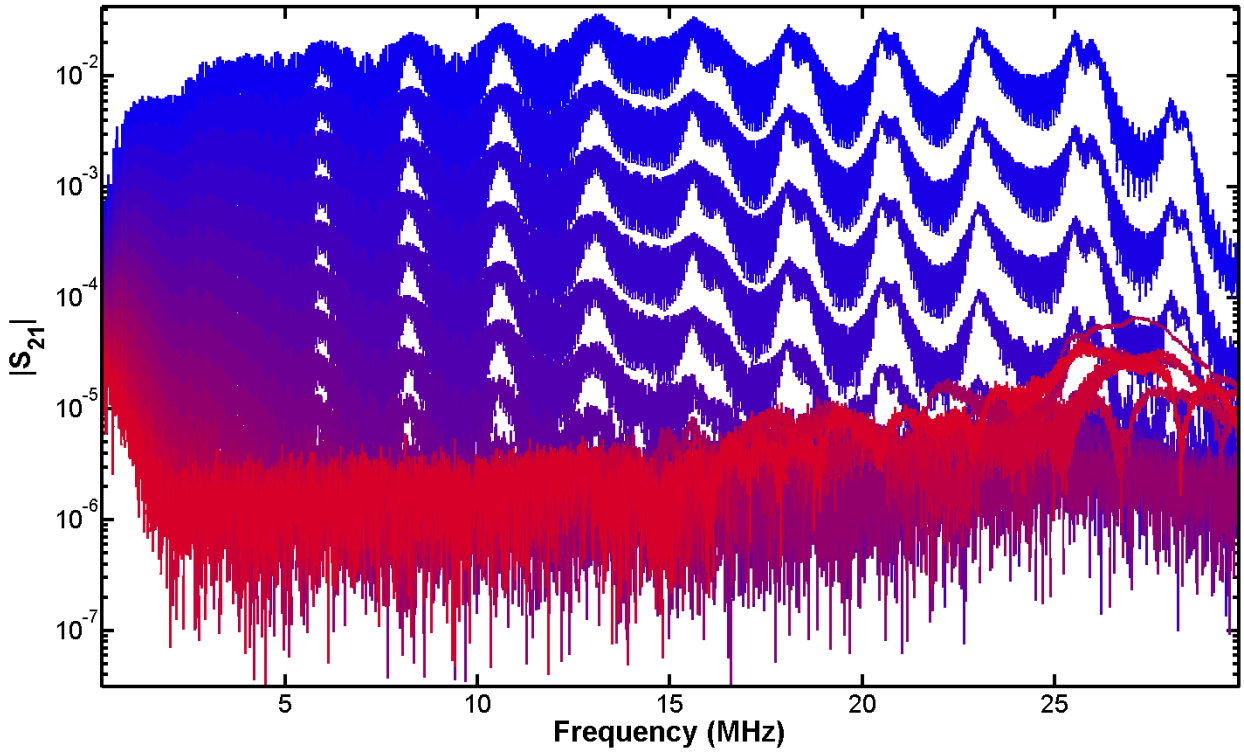

Figure 9. SFAI spectra collected using between 20 and 15,020 feet of coaxial cable.

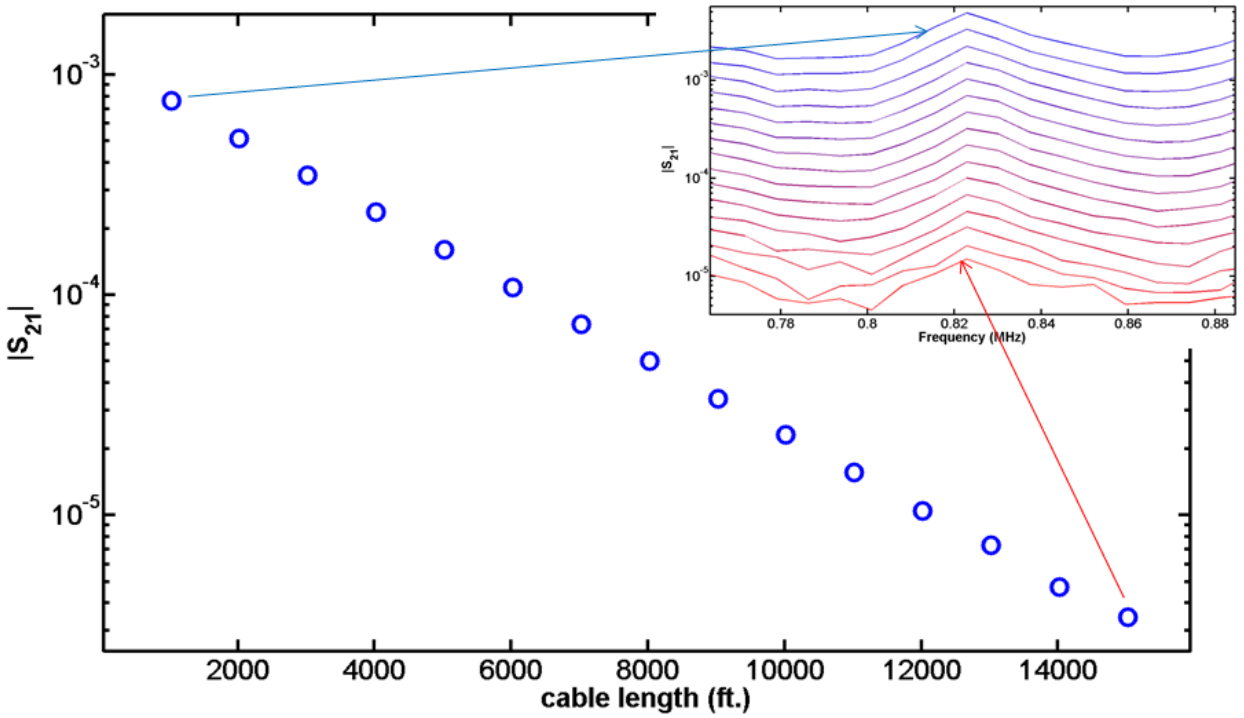

Figure 10. Magnitude of 840 kHz resonance vs. cable length

2. Theoretical modeling and algorithm development

Developed Matlab code for modeling of sound propagation in fluids contained in a rectangular cylinder. One example is shown below, for water and 6% salt solution.

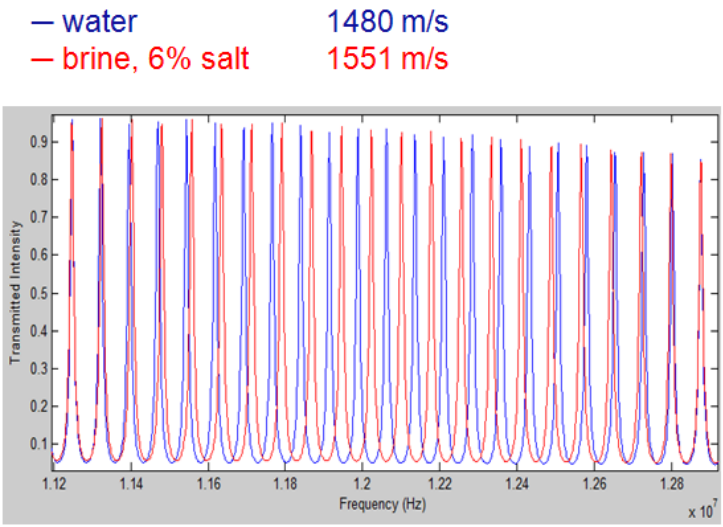

Figure 11. Modeling of sound propagation in H_2O and brine in a rectangular cylinder. Larger differences between resonance peaks correspond to larger sound speeds

Developed two different algorithms for sound absorption determination and coded in Matlab:

(i) One is based on the resonance peak width dependence with absorption, see Figure 12 and Figure 13.

(ii) The other one is based on dependence of the spectral ratio of the one-way travel time and three-way travel time with absorption, Figure 13.

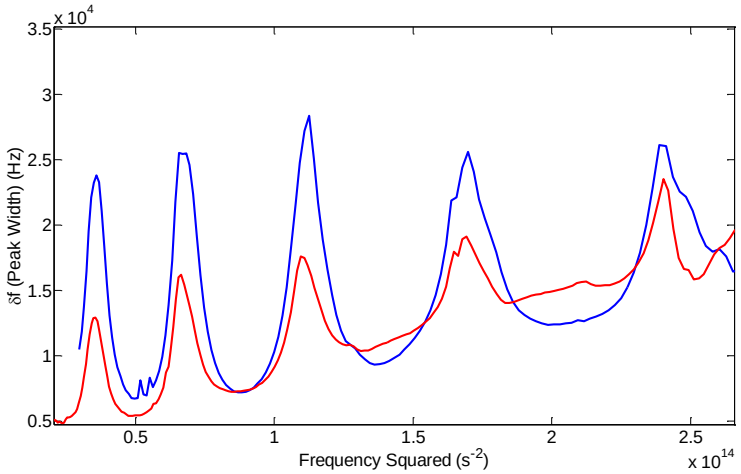

Figure 12. Resonant peak width vs. frequency gives information about acoustic attenuation.

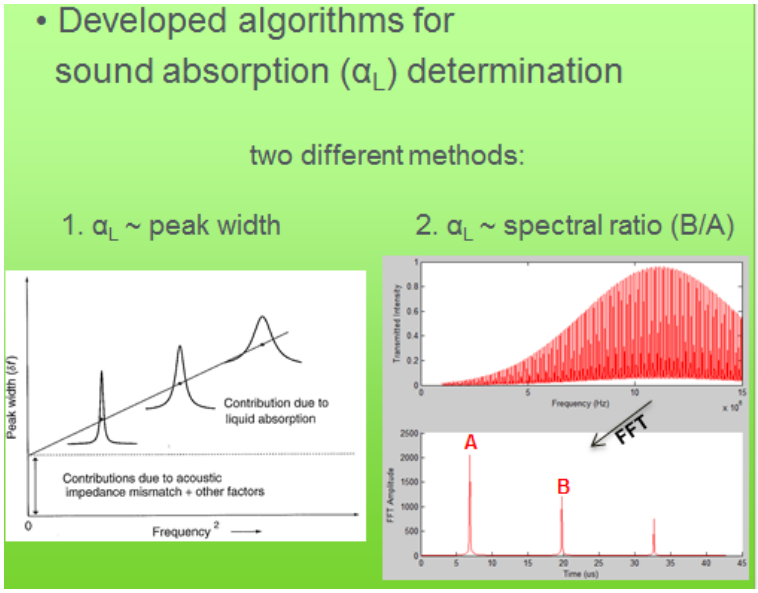

Figure 13. Illustration of algorithms used for sound absorption determination.

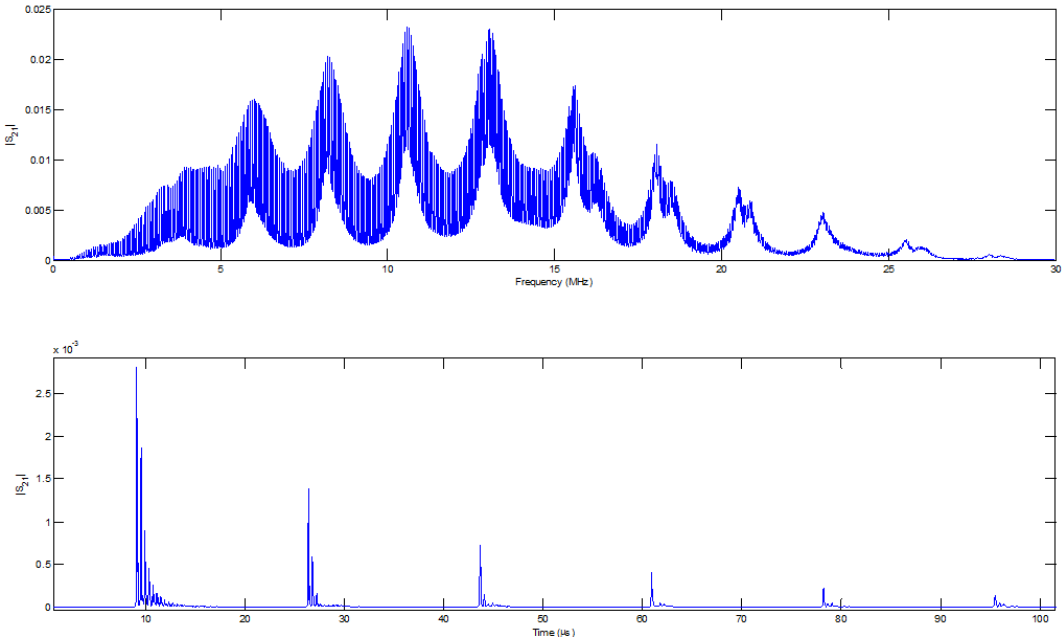

Figure 14. Frequency-domain (top) and time-domain (bottom) spectra for the method based on dependence of the spectral ratio of the one-way travel time and three-way travel time.

The basic idea of the method based on dependence of the spectral ratio of the one-way travel time and three-way travel time consists of: (i) transforming the spectrum to the time domain, Figure 14, (ii) time gating the signal so one has one data set representing a single transit and another representing the triple transit, (iii) converting these data sets back to the frequency domain, Figure 15, (iv) plotting

the ratio of the power spectra, Figure 16, and (v) fitting the resulting data with a straight line, Figure 16, the slope of which is proportional with sound absorption in the medium of interest:

$$\ln\left(\frac{spectrumB}{spectrumA}\right) = -2\alpha L f^2 + \ln(R^2)$$

The line fit of the spectral ratio is given in Figure 16, resulting in good agreement with literature data (α/f^2: 0.108 current experiment vs. 0.092 literature, in $m^{-1}MHz^{-2}$).

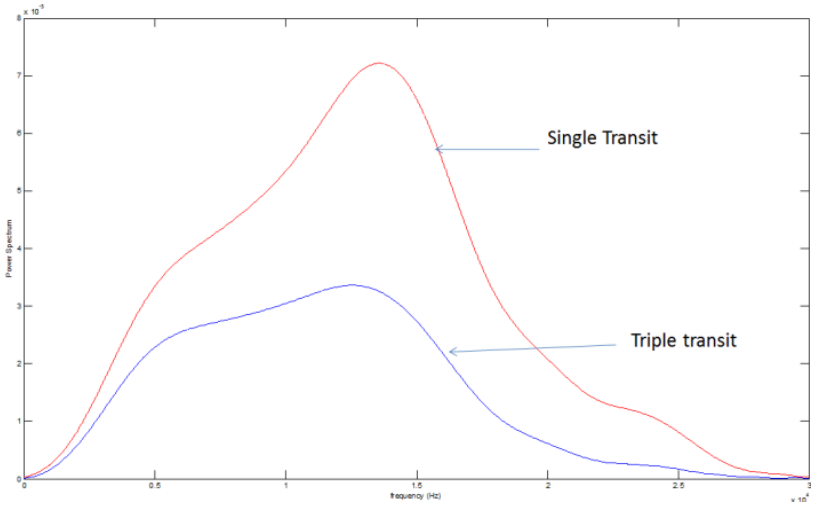

Figure 15. Power spectra of isolated pulses.

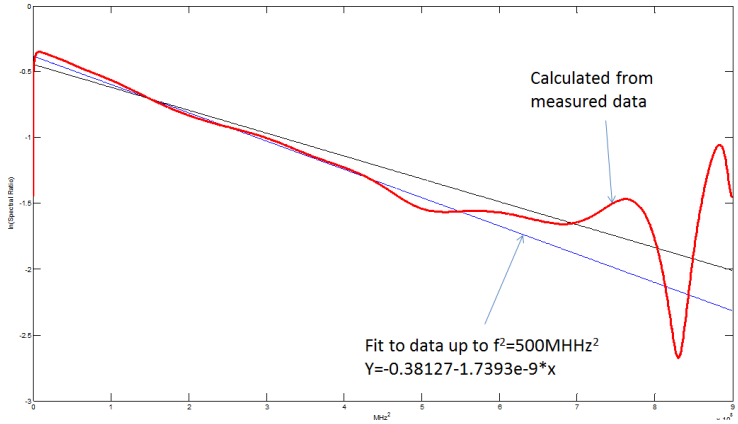

Figure 16. The ratio of the power spectra.

3. Sensor geometry

Preliminary theoretical investigation of rectangular and cylindrical geometries was performed. A good agreement between the experimental data and the theory was observed. Further refinement of the final design proceeded in several steps. Figure 17 shows the two geometries investigated, together with the equations governing the sound speed determination. While the rectangular geometry is relatively

straight-forward, the cylindrical geometry standing-waves formation is described by Bessel functions, and the equation for sound speed determination is valid only for frequencies higher than a threshold value.

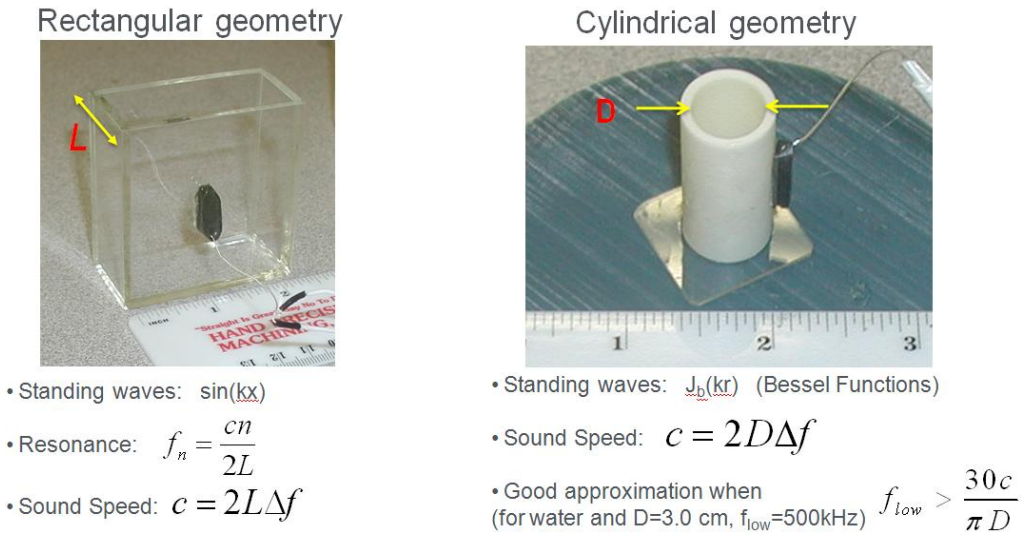

Figure 17. Sensor geometry.

Additionally, investigated rectangular alumina cylinders (custom from McDanel Ceramics), Figure 18 and Figure 19. Investigated high temperature bonding materials, identified electrically insulating adhesive that withstands harsh test conditions, acquired several promising candidates for electrically conductive adhesives, and investigated direct metal-to-metal wirebonding for electrical connections.

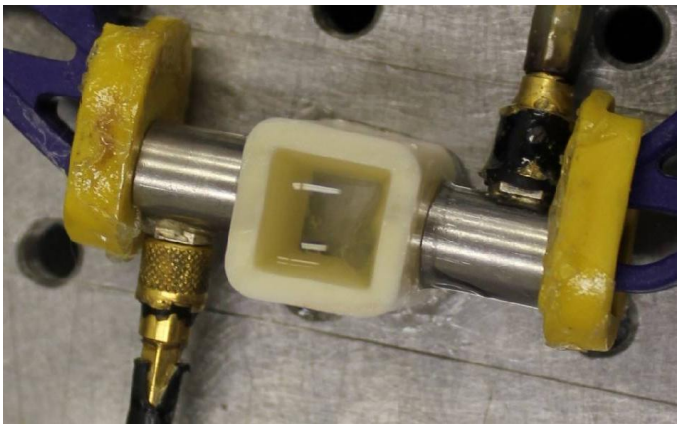

Figure 18. Preliminary tests with a rectangular alumina cylinder resonant cavity.

Experimented with lithium niobate transducers mounted on both inside and outside of cylinder, Figure 19. Tests for survivability up to 374ºC, 22 MPa (3200 psi).

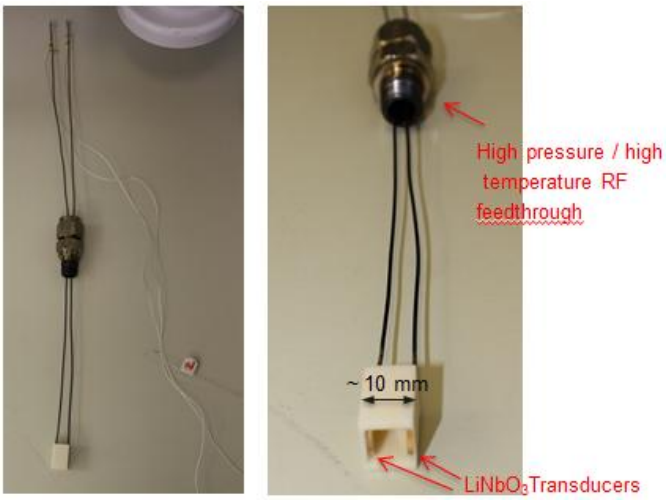

Figure 19. Acoustic Interferometry cell

Experimented with lithium niobate transducers mounted on different sensor geometries. Temperature/pressure range: 270ºC/22 MPa.

The final design resulted in a novel ruggedized sensor constructed from Swagelok compression fittings and ConFlat flanges. Protects transducer crystal, thin-film electrodes and sensitive electrical connections from harsh temperatures and corrosive fluids.

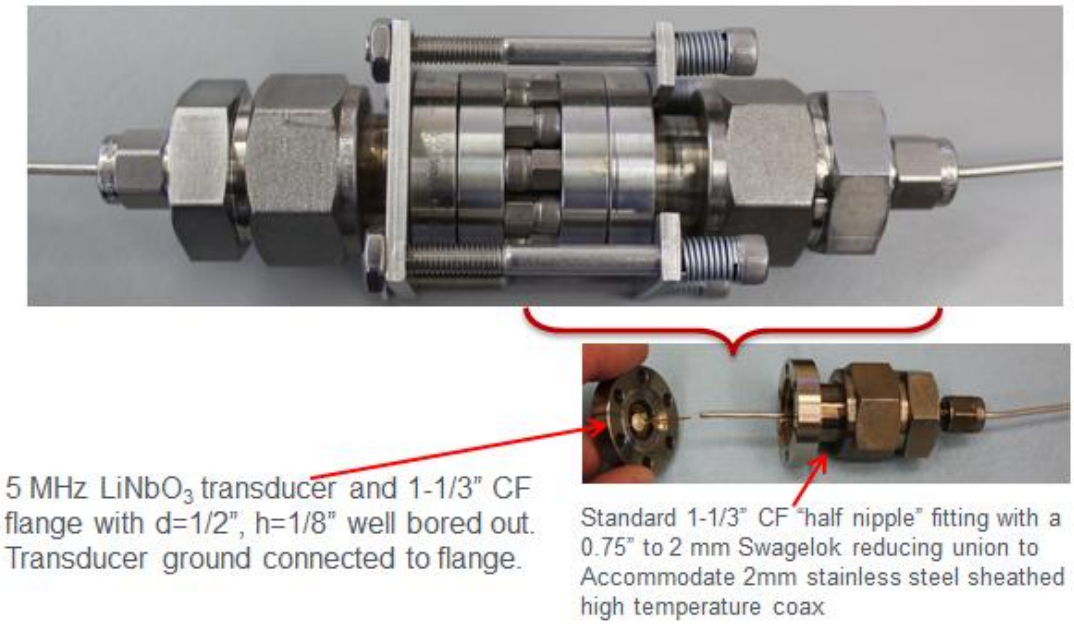

Figure 20. Novel ruggedized sensor constructed from Swagelok compression fittings and ConFlat flanges.

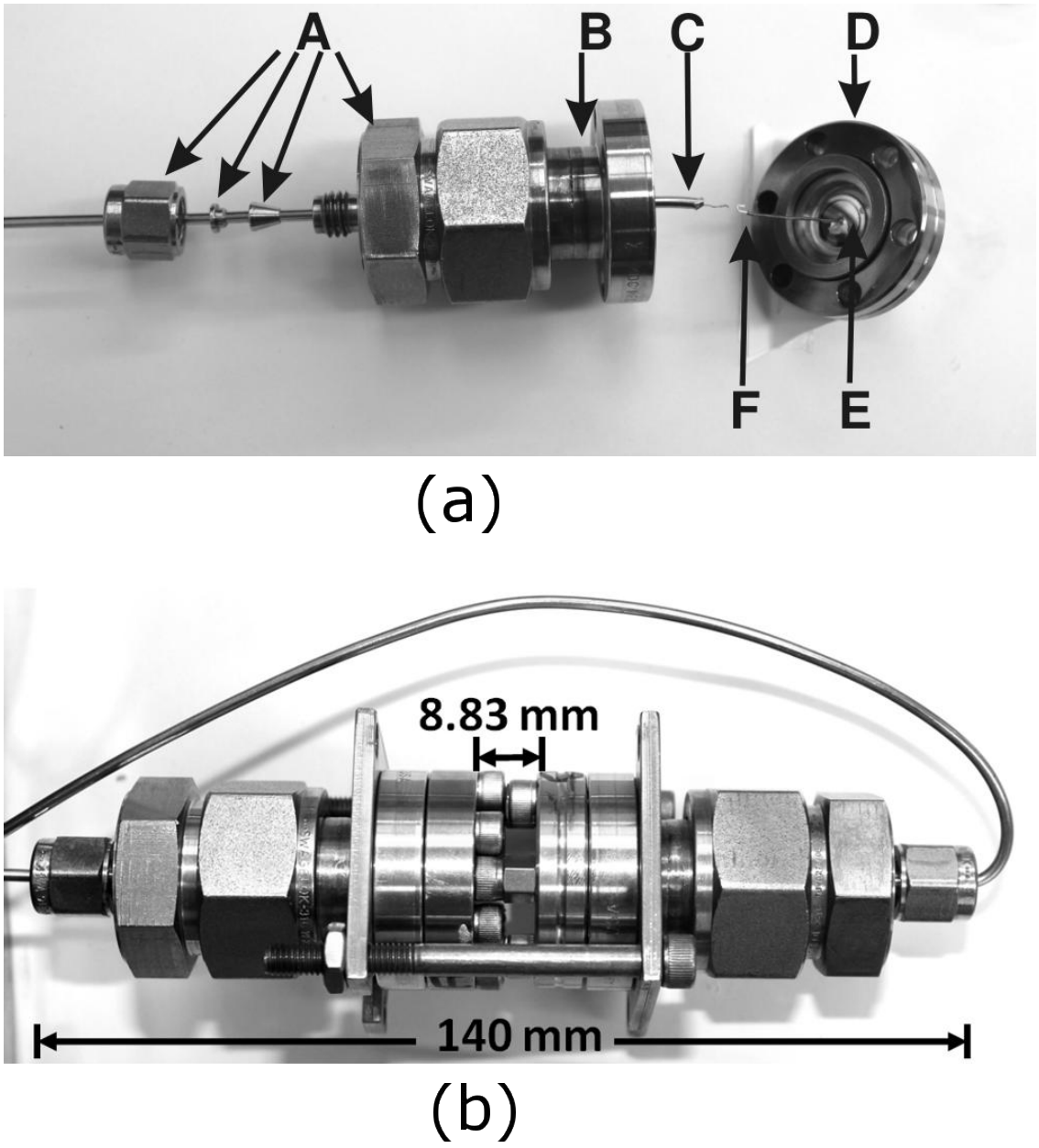

Figure 21. a) The construction of a packaged high temperature and pressure acoustic transducer including a 2 mm-0.75" Swagelok union (A), 1-1/3" Conflat half-nipple (B), high temperature stainless steel sheathed coaxial cable (C), 1-1/3" Conflat blank flange with a custom well 3.2 mm deep x 12.5 mm in diameter bored out (D), a 5 MHz 36° Y-rotated lithium niobate transducer (E), and a flexible Kapton insulated wire (F) for making the connection between the coax center conductor and the transducer. b) Two packaged transducers arranged opposing each other for transmission mode SFAI measurements. The length, L, of the resonant cavity is defined by the bolt heads with spacers used to hold the CF flange together. The measurement cell is compact at 14 cm in length.

This section describes in detail the materials used and the procedure of constructing an SFAI cell for use in high temperature and/or high pressure environments. The piezoelectric elements of the measurement cell (the 'transducers' in Figure **20**) consist of two lithium niobate ($LiNbO_3$) crystals with 5 MHz fundamental frequencies (Boston PiezoOptics, Inc., Bellingham, MA). Lithium niobate was chosen over common alternatives because it has significantly higher piezoelectric coupling than quartz and, with a Curie temperature of 1210°C, is operable at significantly higher temperatures than lead zirconium titanate (PZT). The 36° Y-rotated cut of lithium niobate having "Z-Y'-Z'' convention" Euler angles (90°, -36°, 0°) was chosen because it excites a pure-longitudinal acoustic mode. No shear component was desired since the cell is used to study fluids. The 10 mm diameter crystals were metalized with Cr/Au in a standard coaxial configuration and had an active area 7 mm in diameter.

To protect the transducers from mechanically and chemically harsh test environments, a stainless steel package was constructed using commercially available Swagelok and Conflat (CF) fittings. A well was bored in 1-1/3" CF blank flange to accommodate a single lithium niobate transducer (see Figure 21a). The well had a diameter of 12.5 mm, a depth of 3.2 mm, and a bottom surface that was smooth and parallel to the front face of the flange to within 25 μm. Most gels that are commonly used to acoustically couple piezoelectric transducers to other components of a system are water-based and thus unsuitable for use at the target temperature of 250°C. For the HTP-SFAI cell, a number of high temperature organic and ceramic-based adhesives were tested to acoustically couple the transducer to the CF flange with differing degrees of success. Some of the adhesives tested formed voids due to outgassing during the curing process which significantly degrades the ability to transmit ultrasound. Other adhesives had coefficients of thermal expansion that were drastically different than that of the transducers and caused excessive stress, sometimes resulting in destruction of the transducer, at higher temperatures. Ultimately, the best acoustic couplant in terms of high temperature stability and efficiency of ultrasound transmission was a commercially available specialty high temperature epoxy (Epoxy H24 from Epoxy Technologies, Inc., Billerica, MA). The CF blank is mated to a 1-1/3" half nipple and sealed using a copper gasket capable of withstanding >250°C. The half nipple is connected to a 0.75" to 2 mm Swagelok reducing union as shown in Figure 21a. The 2 mm end of the Swagelok reducing union accommodates a high temperature (~600°C) stainless steel-sheathed coaxial cable (THERMOCOAX, Inc.) that is used to transmit the signal to and from the cell. The stainless steel sheath of the coaxial cable protects the copper center conductor from mechanical or chemical damage while the mineral powder dielectric allows this cable to be used well above the 250°C temperature required for this application. Because the coaxial cable is rigid, a flexible Katpon insulated wire was

used to connect the coax center conductor to the transducer. This flexibility of this wire allows the Swagelok and Conflat assembly to be sealed after all electrical connections have been made. Electrical connections between the coaxial cable and the transducer were made using a high temperature silver-filled epoxy (E4110-LV, also from Epoxy Technology, Inc.). This epoxy was chosen because it was found to maintain a low resistivity and showed little degradation in preliminary furnace tests up to 400°C. Two of the stainless steel packaged transducers shown in Figure 21a were arranged facing each other (Figure 21b) with the front faces of the CF blanks defining the boundaries of the SFAI cell. On one transducer package, the CF blank flange was fastened to the CF half nipple using six standard ¾" long bolts. On the other transducer package, the CF blank flange was fastened using three ¾" long bolts and three bolts which included an additional spacer, one of which can be seen in Figure 21b. The three bolts with the additional spacers define the physical dimension of the resonant cavity, L.

Electrical connections: 1) between lithium niobate ground and flange and 2) between lithium niobate center conductor and coax cable center conductor all made with silver epoxy. All electrical connections and epoxies are completely sealed off from aqueous environment. Thick stainless steel walls provide protection against collapse under high pressure (tested up to 3000 PSIG so far).

4. Flow Measurement and Fluid Composition

Flow measurements were performed using a two-stage geometry, in which two pairs of facing transducers are excited with a train of pulses. Different vortices, bubbles, solid particles present in the flowing fluid can block the acoustical signal to go through the region of interest. The recorded waveforms can be analyzed relatively easy, as the flow rate is proportional with the distance L between the pairs of transducers and the time between the two blocked-signal regions.

The concept for flow measurements and collected data for water flow in an in-house flow-loop, at room temperature are shown in Figure 22. There is a very good agreement between our flow data and a Coriolis meter, which is the oil/geothermal industry standard for flow determination. The main advantage of our approach is that our sensor can be used at elevated pressure and temperature.

Sound speed determination was performed using the SFAI technique. In a typical SFAI spectrum, Figure 23, three sets of resonances can be seen. The resonance of the 5 MHz lithium niobate transducers dominates the overall power distribution of the measurement cell; The SFAI cavity walls have their own resonances with ~800 kHz spacing, shown by the gray envelope. Finally, the fluid resonant peaks, spaced at ~80 kHz, are seen throughout the entire spectrum.

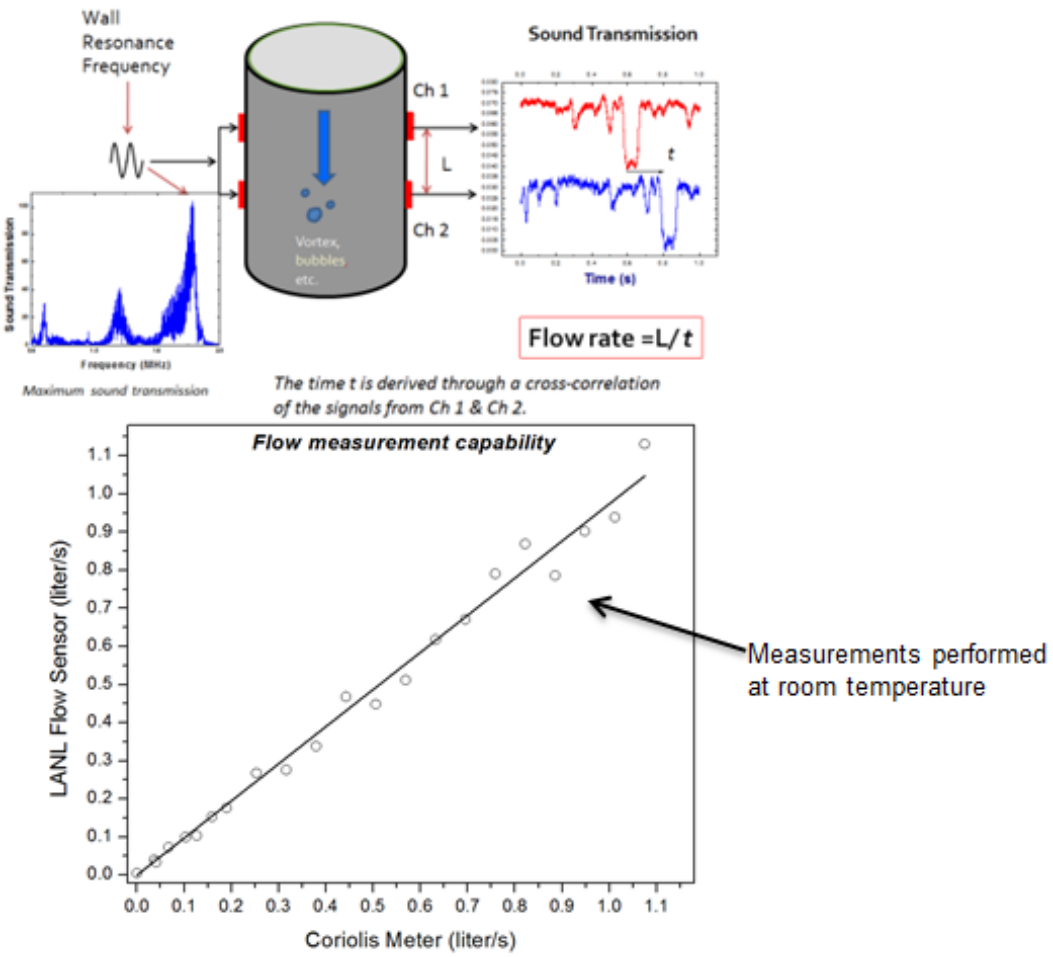

Figure 22. Flow measurement concept and data.

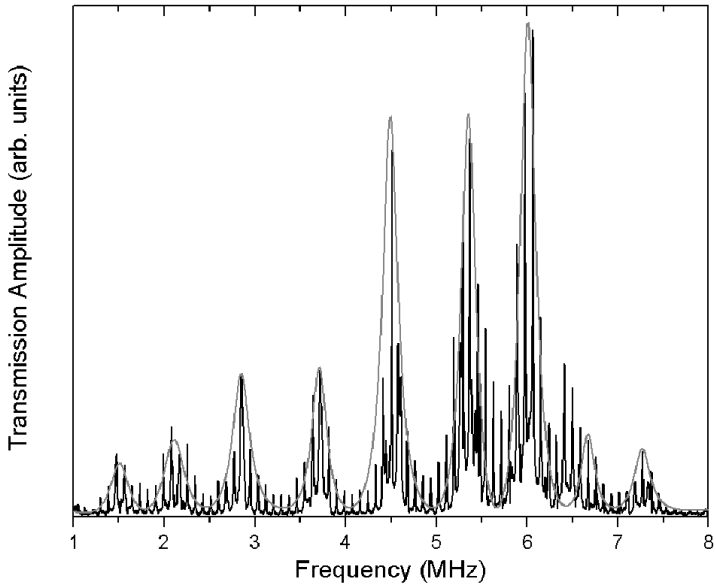

Figure 23. A typical SFAI spectrum

Examples of typical experimental data collected at different temperatures are shown in Figure 24 and Figure 25.

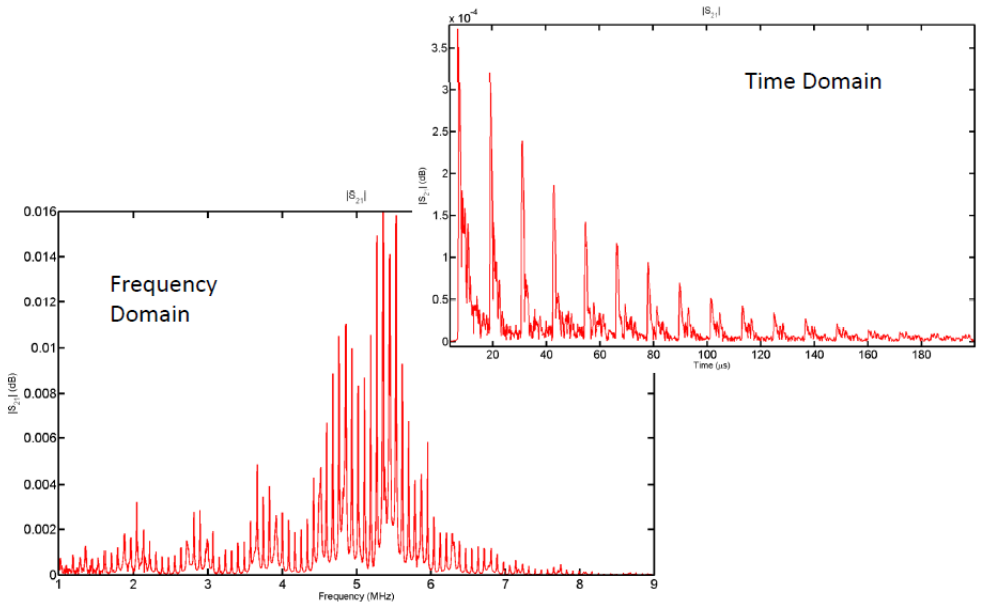

Figure 24. Transmission Data @ 26 °C.

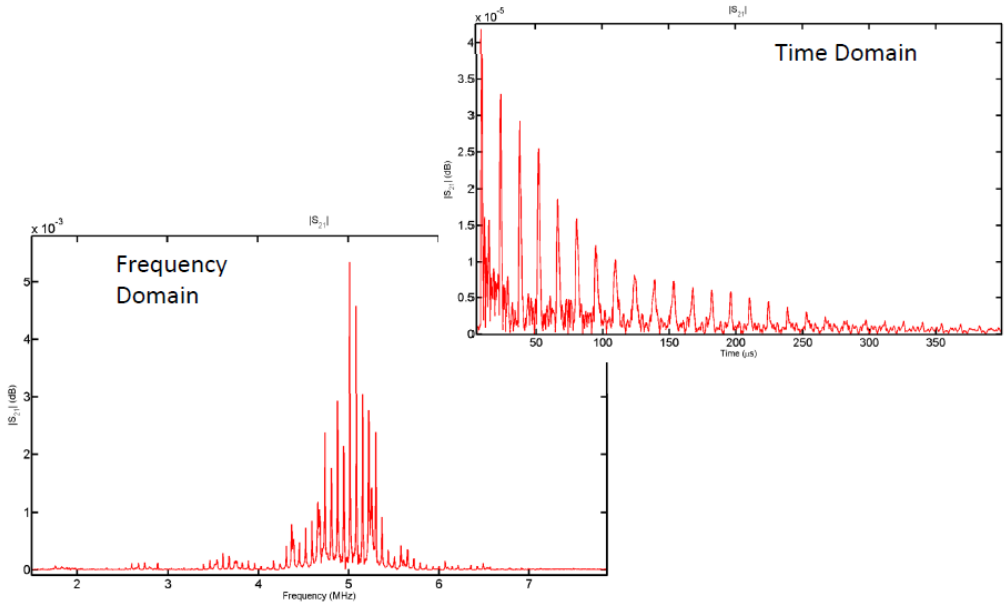

Figure 25. Transmission Data @ 226 °C.

In a slightly different configuration, data can be collected in reflection mode, see Figure 26. The main advantage of such an approach is that a single transducer can be used, instead of a pair of two facing transducers. However, the disadvantage is that the central resonance of the transducer is

dominating the spectrum, and the peaks for the fluid of interest might be more difficult to extract from the spectrum.

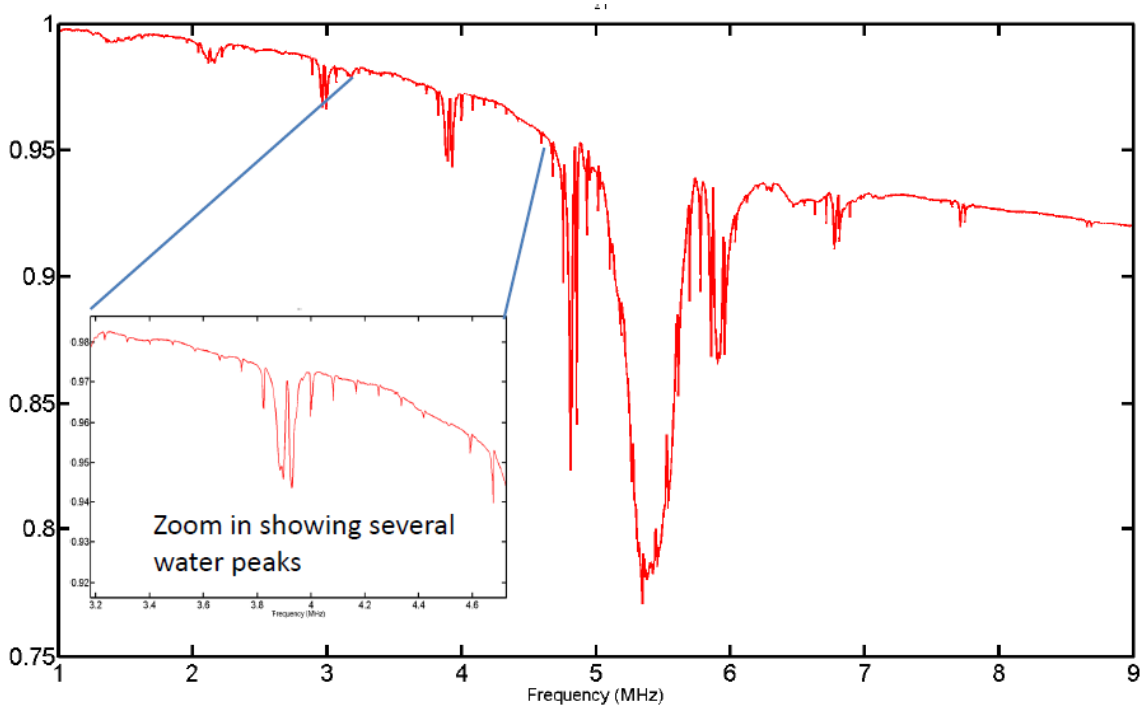

Figure 26. Reflection Data @ 26 °C

The next three paragraphs (A,B,C) are excerpts from 'An Acoustic Resonance Measurement Cell for Liquid Property Determinations up to 250°C', LA-UR-12-24498. Blake Sturtevant, Cristian Pantea, Dipen Sinha accepted in *Review of Scientific Instruments*. So are a few other sections in the report.

A. Determining Sound Speed from $|S_{21}|$ Spectrum

Figure 27a shows a representative plot of the transmission scattering parameter, $|S_{21}|$, vs. frequency, collected at 30°C and ambient pressure. Many fluid resonance peaks can be identified from such a plot. 25 of these resonances, chosen because they are apart from wall and transducer resonances as described in Section II, are indicated with circles in the figure. To determine df_n/dn, the frequencies of the resonances identified in Figure 27a are plotted against 'cycle number' while taking care to account for cycles for which resonances are not recorded (specifically: n=[5-7, 13-15, 22-25, 32-36]) as shown in Figure 27b. For the purpose of determining sound speed, it is only necessary to know *n* in a relative and not an absolute sense since the slope of f_n vs *n* is the only quantity of interest. A linear least squares fit, shown in Figure 27b, can be performed on the data to determine df_n/dn. For the 25 resonances shown in Figure 27, a least squares fit determined $\frac{df_n}{dn}$=85.408±0.033 kHz. Using a measured path length, L=8.848 mm, the sound speed is determined to be 1511.4±0.6 m/s. The standard deviation, σ=33 Hz, of

the linear fit slope is reported as the uncertainty here. This uncertainty contributes to a relative uncertainty in sound speed of 0.04%.

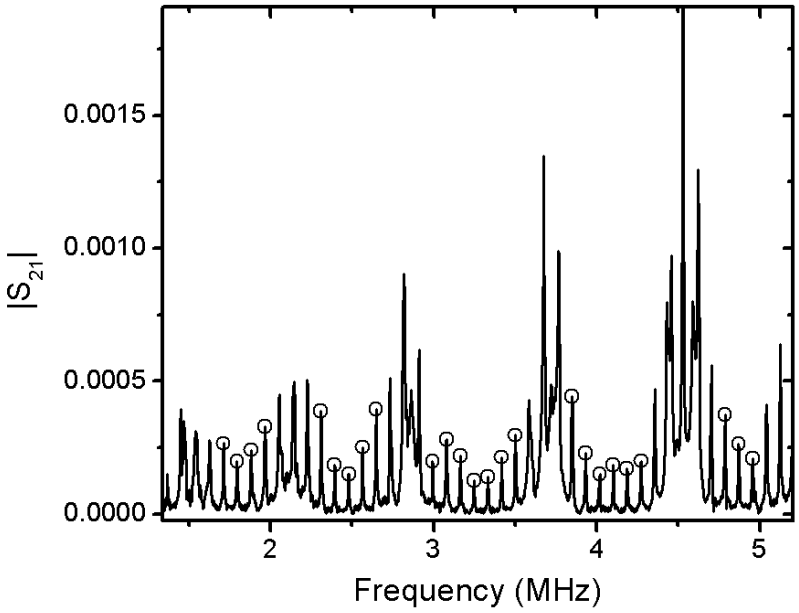

(a)

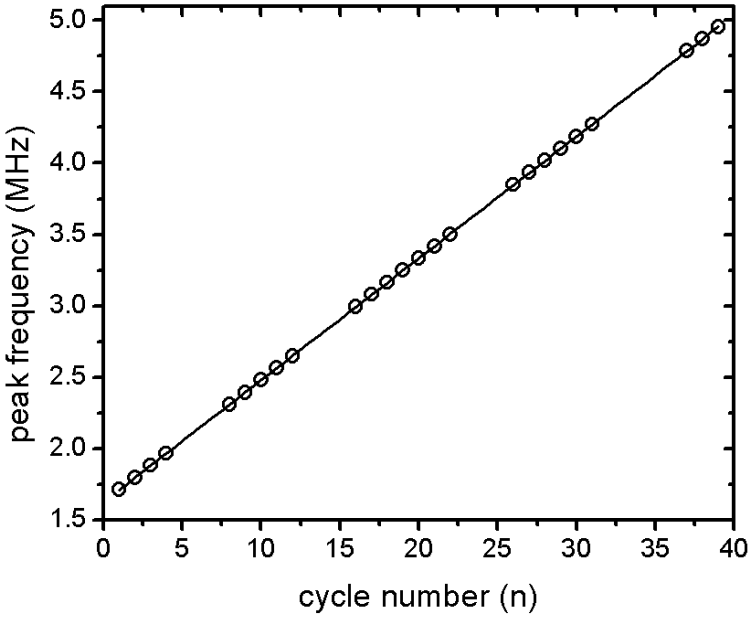

(b)

Figure 27. a) The center frequency of 25 f_n, indicated with open circles, in regions not affected by wall or transducer resonances, were selected for computation of df_n/dn. b) These center frequencies plotted vs *n*, with skipped cycles accounted for and a linear fit shown.

B. Sound Speed as a Function of Pressure at 31°C

The first set of data presented here was collected at 30.9±0.5°C at 20 pressures between ambient pressure and 3000 psig. Table 2 presents the determined sound speed vs. pressure data along with the sound speed calculated by the IAPWS-IF97 standard. The IAPWS-IF97 sound speeds are not experimental points, but are calculated from the equation of state for water. The equations used in these calculations can be found in the IAPWS-IF97 standard, while the full set of experimental thermodynamic data upon which the equations of state is based are given in a reference within. The IAPWS calculations are used for comparison since there is no single set of direct sound speed measurements over the entire temperature and pressure range reported here. To determine the sound speed from a measured transmission spectrum, df_n/dn was calculated as described in the previous section. The path length, L=8.848 mm, was calibrated using deionized and degassed 25°C water as a standard. As a result of the test environment described previously, pressure changes were accompanied by small changes in temperature due to compression or expansion of the gas in the headspace of the vessel. Because an increase in temperature of 1°C has the same effect on the sound speed in water as increasing the pressure by 200 psi, the slightly different temperatures had to be accounted for when comparing measurements against predicted values. In all cases, the determined sound speeds agree with the IAPWS-IF97 values to within 0.5 m/s. This agreement provides a validation for the measurement precision determined by the linear fit of f_n vs n.

Table 2. Comparison of experimentally determined and predicted sound speed

Temp (°C)	Pressure (psig)	Determined Sound Speed (m/s)	Predicted Sound Speed (m/s)
30.4	7	1511.8	1512.0
30.4	195	1513.7	1514.0
30.5	397	1516.1	1516.3
30.4	600	1518.4	1518.5
30.5	797	1521.0	1520.9
30.6	999	1523.0	1523.4
30.6	1205	1525.4	1525.6
30.7	1400	1528.1	1528.0
30.7	1606	1530.2	1530.3
30.8	1798	1532.9	1532.7
30.9	1997	1534.8	1535.1
31.0	2195	1537.2	1537.6
31.2	2402	1540.1	1540.4
31.3	2602	1543.0	1542.8
31.4	2813	1544.9	1545.4
31.4	2995	1547.2	1547.5

C. Liquid Water Sound Speeds Measured Along the Liquid-Vapor Coexistence Curve

The second set of data presented here was collected in liquid water at 22 temperatures between laboratory ambient and 250°C at pressures corresponding to the liquid-vapor coexistence line. At each temperature, the sound speed was determined using the procedure described above. The path length, L, was corrected for changes in temperature using a calibrated 25°C value of L and a linear thermal coefficient of expansion for stainless steel of 16×10^{-6}/°C. The measured data show very good agreement with the IAPWS-IF97 predicted sound speeds as can be seen from Figure 28 and Table 3. For all points, the discrepancy between the measured and IAPWS-IF97 predicted sound speed is better than 0.3% (~3 m/s). The discrepancies are likely attributed to errors in the temperature measurements by the thermocouple. At higher temperatures especially, a small error in temperature can have a significant impact on the sound speed of water. For example, at 220°C, a change in temperature of 1°C leads to a 3.6 m/s change in water sound speed. The inability to measure temperature to better than about one degree Celsius reflects limitations of the present test environment and does not affect the measurement precision of the HTP-SFAI measurement cell. As indicated above and in Table 2, the precision of the measurement cell is better estimated by the standard deviation in df_n/dn and is typically in the range of 0.5 m/s or better.

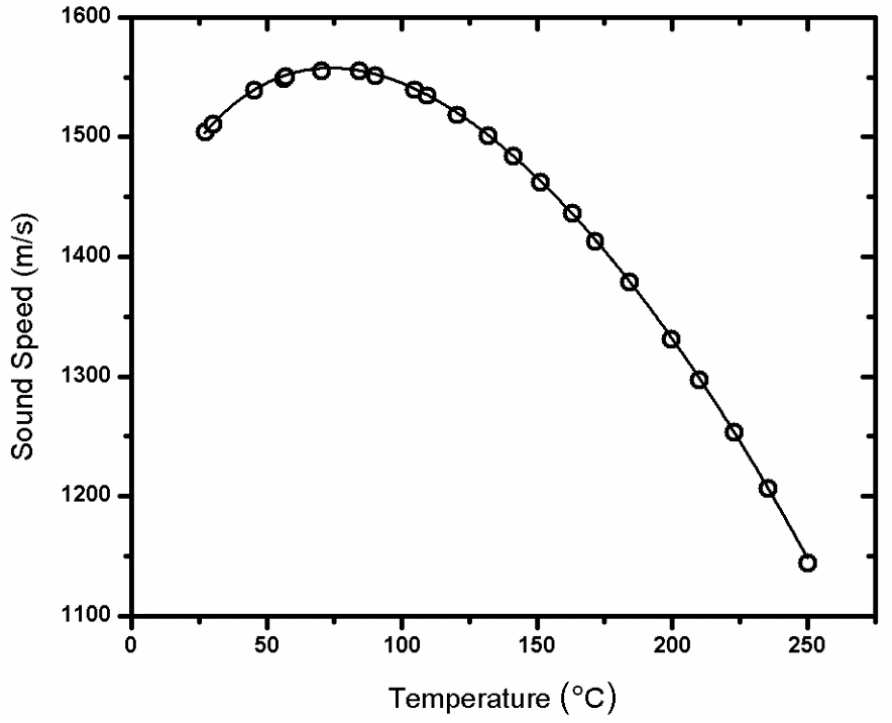

Figure 28. The speed of sound in water up to 250.4°C along the liquid-vapor coexistence curve. The 22 open circles represent sound speeds determined from SFAI measurements while the solid trace corresponds to sound speeds calculated from IAPWS-IF97 standard.

Table 3. Experimentally determined and predicted water sound speeds along the liquid-vapor coexistence curve

Temperature (°C)	Determined Sound Speed (m/s)	Predicted Sound Speed (m/s)	Difference [a] (%)
27.5	1504.4	1504.7	-0.02
30.3	1510.2	1511.5	-0.09
45.5	1538.5	1539.6	-0.07
56.5	1548.7	1551.3	-0.17
57.3	1549.9	1551.9	-0.13
70.4	1555.2	1557.5	-0.15
84.5	1555.0	1555.5	-0.03
90.3	1551.1	1552.5	-0.09
104.8	1539.1	1540.3	-0.08
109.6	1534.3	1534.9	-0.04
120.5	1518.0	1520.3	-0.15
132.1	1500.6	1501.3	-0.05
141.4	1483.4	1483.9	-0.03
151.4	1462.1	1462.9	-0.05
163.1	1436.0	1435.7	0.03
171.6	1412.9	1414.1	-0.09
184.4	1378.7	1378.8	-0.01
199.8	1331.1	1332.1	-0.08
210.1	1297.1	1298.3	-0.10
223.1	1252.8	1252.8	0.00
235.6	1206.2	1206.0	0.01
250.4	1143.6	1146.7	-0.28

a. Difference=100* (Measured-Calculated)/Measured

We reported here a new measurement cell that can be used for resonance-based sound speed measurements in fluids up to temperatures of 250°C and pressures of at least 3000 psig. The measurement cell is based on the room temperature Swept Frequency Acoustic Interferometry technique but advances the state-of-the-art by using commercially available specialty adhesives and a simply constructed stainless steel housing to equip it for immersion in thermally, mechanically, and chemically harsh environments.

Example sound speed data as a function of temperature and pressure were presented as a demonstration of the measurement cell capabilities. The data were compared to the internationally accepted standard, IAPWS-IF97, and shown to be in very good agreement at temperatures up to 250°C

and pressures up to 3000 psig. The precision achieved with the measurement cell is shown to be significantly better than 0.1%.

The maximum temperature and pressure reached in all the experiments performed in the lab using the newly designed SFAI cell are 270°C and 22 MPa (3500 psi).

Salinity determination

Data for salinity determination were collected at room temperature and pressure. Different concentrations of NaCl in distilled water was used, see Figure 29.

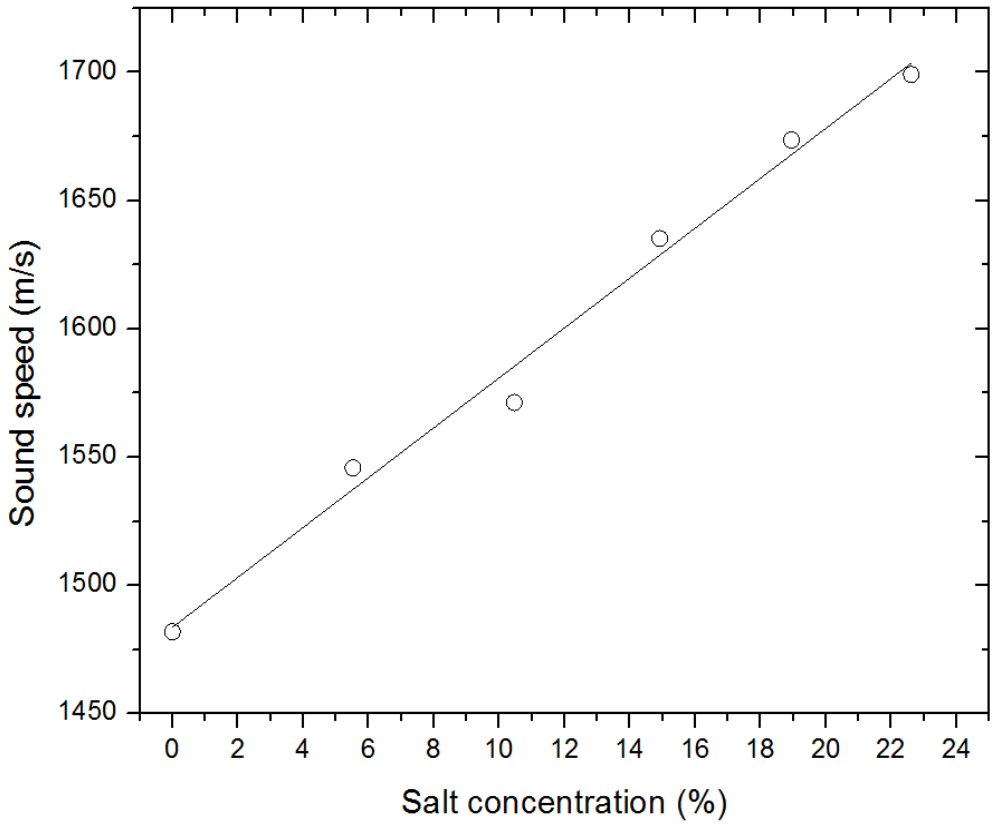

Figure 29. Data for sound speed vs. NaCl concentration in water.

Geothermal-like brines at high pressure and temperature

Two different brines were prepared for determination of the sound speed at high pressure and temperature. The data were collected up to just below 200C, along the liquid-vapor coexistence line.

i) NaCl-based brine

For the NaCl-based brine we used seawater, which was about 32 parts per thousand (total dissolved solids). It was primarily NaCl with other salts and minerals present in much smaller concentration. The data are shown in Figure 30.

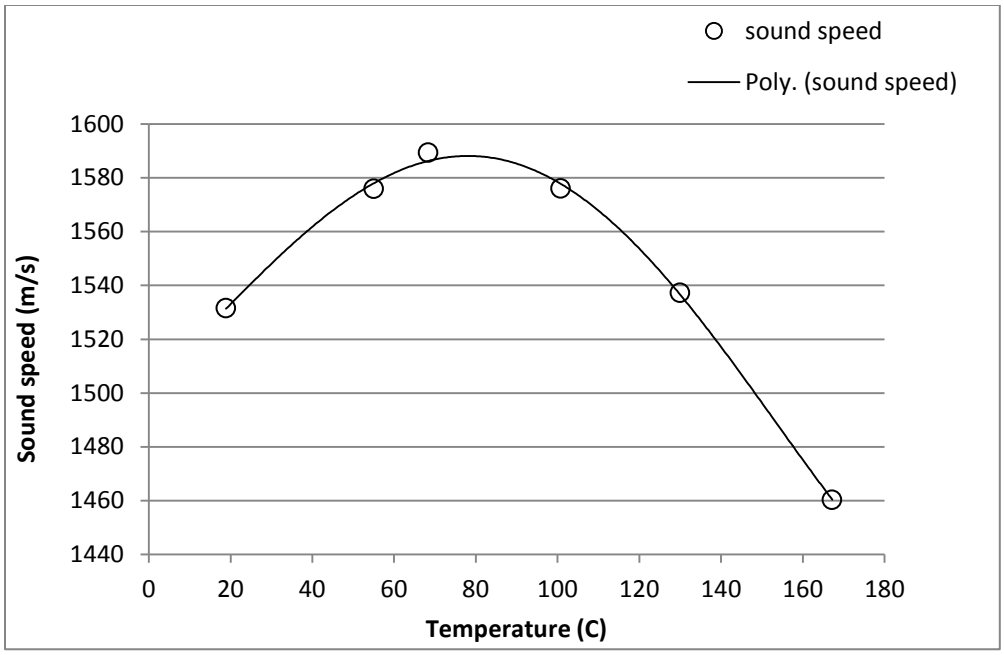

Figure 30. Seawater data along the liquid-vapor coexistence line.

ii) Geothermal brine

The other brine was "HTB1" formulation provided by the Geophysics group at Los Alamos National Laboratory. This is much closer in ingredients/concentrations to real geothermal brines. The description of the ingredients and concentrations is presented in Table 4.

Table 4. HTB1 geothermal brine

Chemical	**mass, g**	**Moles**	**Ionic Strength**	**mg/l**
NaH_2PO_4	0.665	0.0055431	0.011086105	665
$Na_2HPO_4 – H_20$	0.755	0.0028175	0.005642897	755
$NaHCO_3$	1.498	0.0178333	0.035666667	1498
KCl	0.415	0.0055667	0.011133467	415
NaCl	3.481	0.0595552	0.119110351	3481
H_4SiO_4	0.105	0.0010926	0	105
Na_2SO_4	0.053	0.000373	0.000746093	53
18 MΩ Water	1000			
TDS, g/L	6.972			

The data collected at pressures and temperatures typical to geothermal reservoirs are shown in Figure 31.

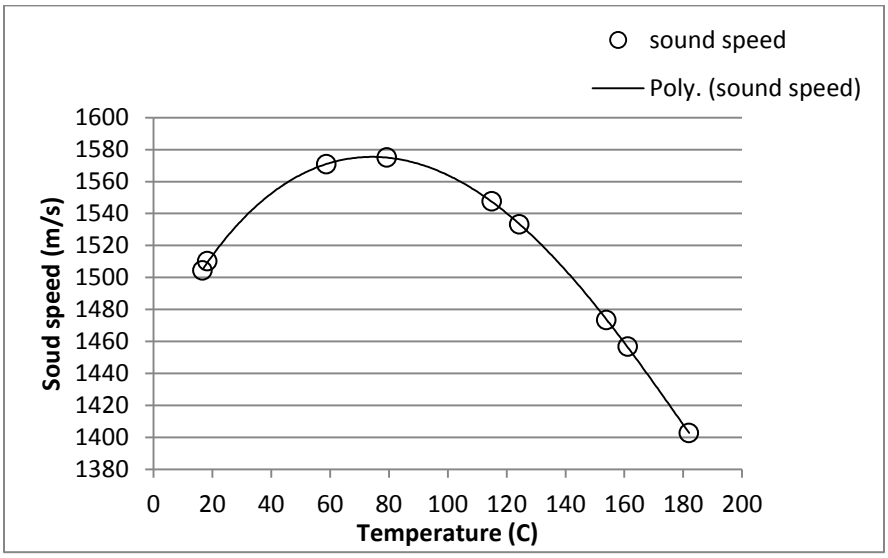

Figure 31. HTB1 brine data along the liquid-vapor coexistence line.

5. *Temperature and pressure calibration*

5.1.1. Temperature Determination

Temperature determination experiments were performed using a Lithium Niobate transducer with a center resonance frequency of 3.5 MHz, with the following dimensions: 15mm x 4 mm x 0.9 (thickness) mm. The HTHF coaxial cable was electrically connected to the transducer using conductive epoxy. The transducer was placed inside a quartz tube in a furnace that was heated up to 430°C. Figure 32 shows the electrical impedance spectrum of the transducer at room temperature. Several lower-modes resonances can be observed in the spectrum (Region I-V, Region VII), along with the center resonance at 3.5 MHz (Region VI).

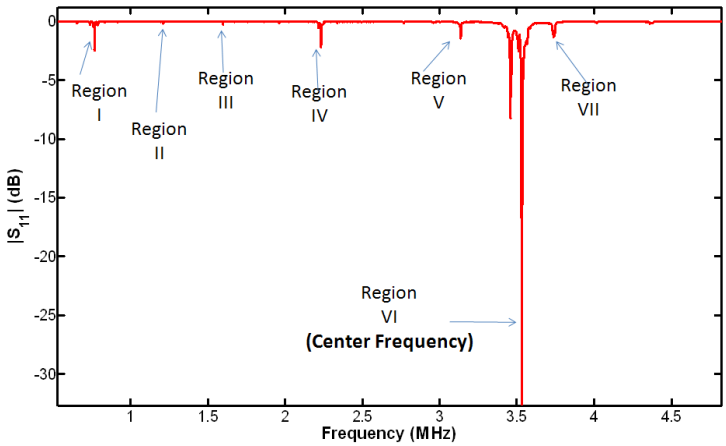

Figure 32. 3.5 MHz Lithium Niobate transducer impedance spectrum.

The obvious choice of center frequency of the transducer behaved in a very strange manner, as several peaks were present in the frequency spectrum with each peak displaying different amount of variation in amplitude and frequency with temperature, see Figure 33 below. The cluttered nature of the frequency spectrum makes peak tracking very difficult, due to the 'messy' nature (several splitting peaks).

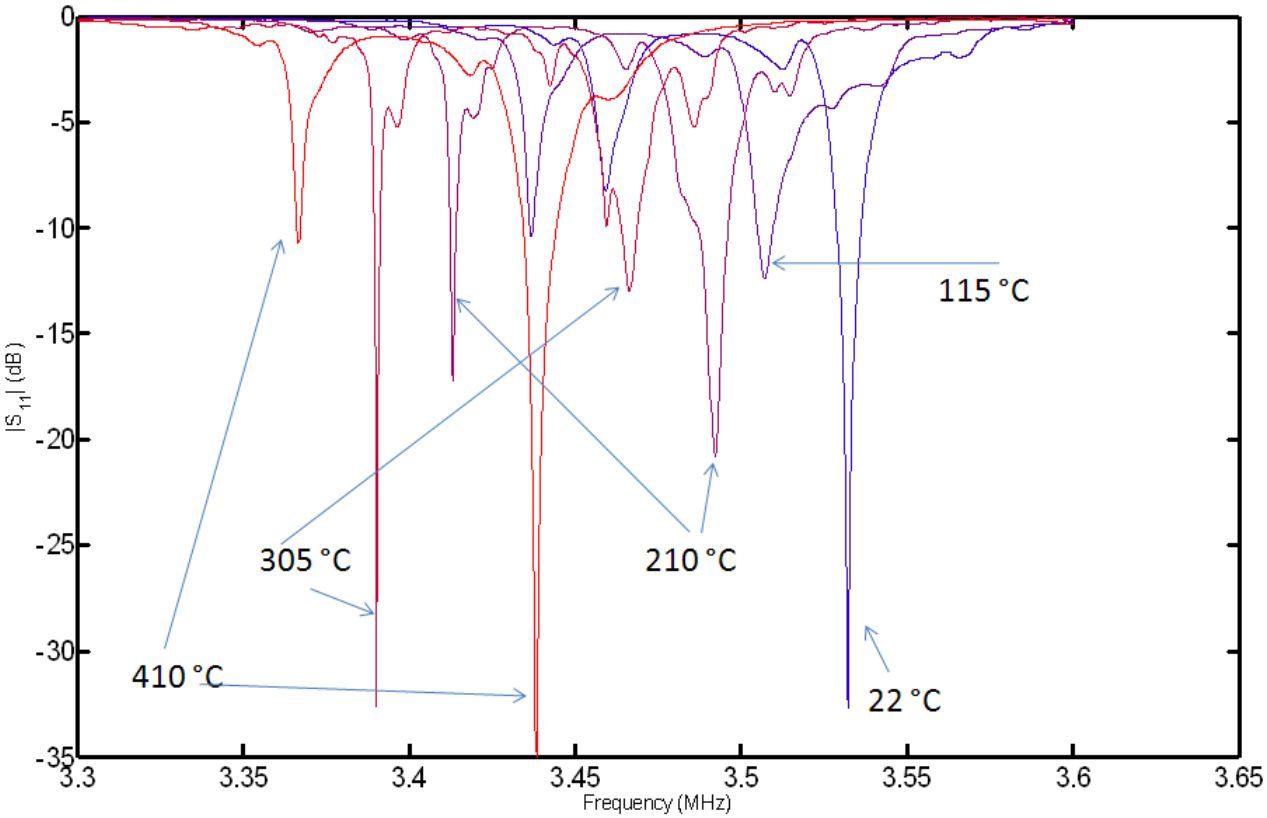

Figure 33. Center frequency dependence with temperature.

Consequently, we decided to investigate a larger part of the frequency spectrum of the transducer while the temperature is varied. The frequency response of each of the regions in Fig. 3 was tracked as the temperature was increased to 430°C, and then decreased back down to room temperature. An example of this measurement is shown in Figure 34, where Region III was investigated more thoroughly. In this case, a much cleaner spectrum was obtained, and the change in frequency of the single peak is very straightforward to track.

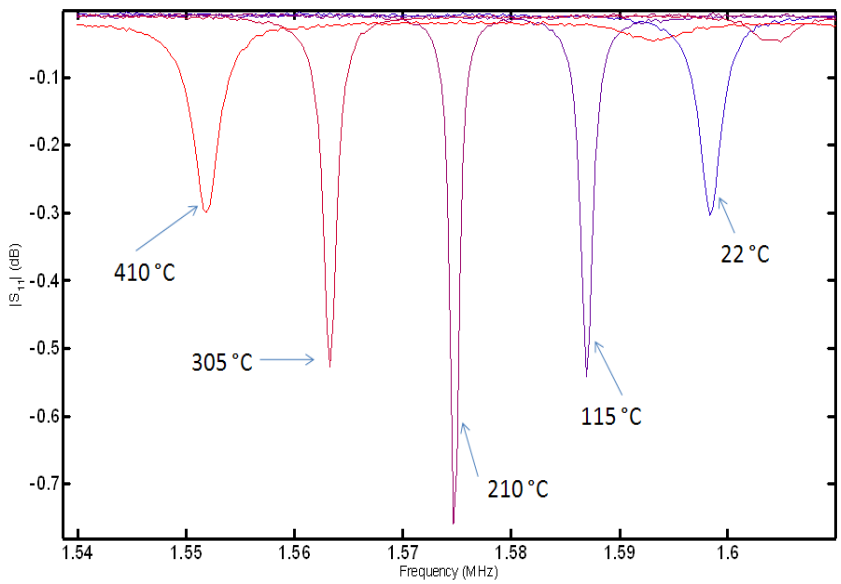

Figure 34. Region III dependence with temperature.

The peak positions determined from the heating and cooling cycles are represented in Figure 35. A very good sensitivity in terms of frequency variation as a function of temperature of 83 ppm/^{o}C was obtained. Additionally, there is no hysteresis between the heating and cooling cycle, and, with the right calibration, the temperature of the reservoir can be precisely determined. This is a major breakthrough for the multipurpose acoustical sensor.

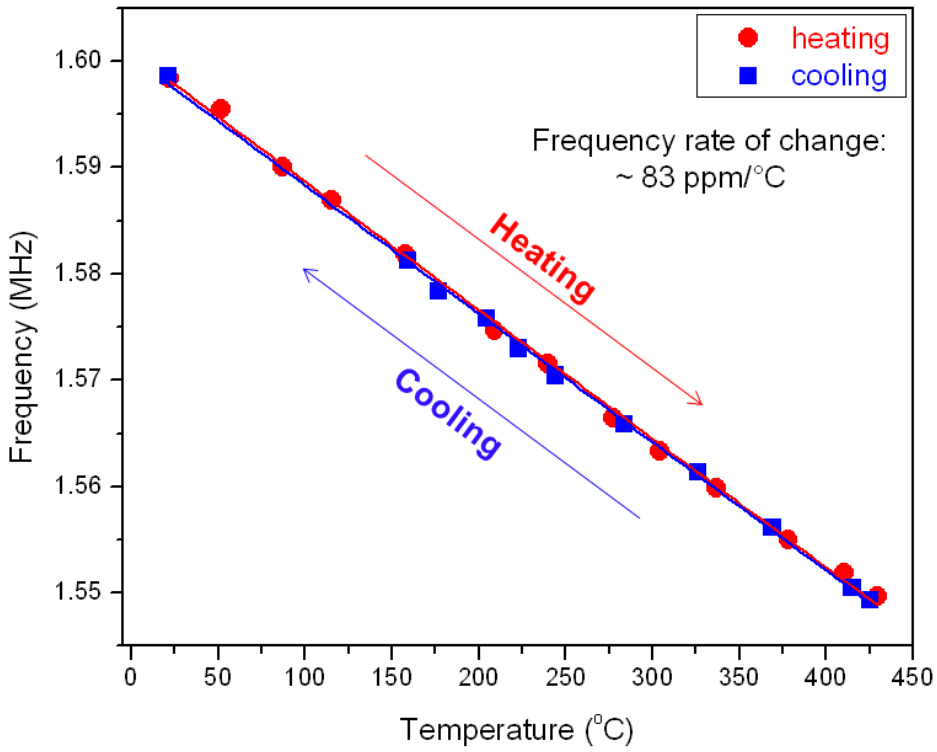

Figure 35. Lower mode (region III) dependence with temperature.

5.2. Pressure Determination

For pressure sensor investigated the following geometries:

- Film Bulk Acoustic Resonator (FBAR): differential pressure → changes stiffness, density film →changes resonant frequency (Chiu et al., Jap. J App. Phys., (46):1392-1397, 2007), Figure 36.

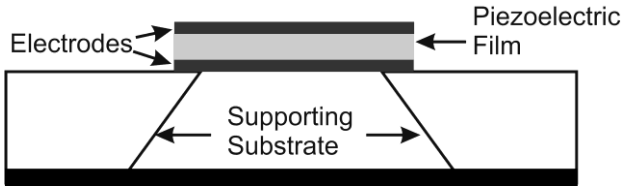

Figure 36. Film Bulk Acoustic Resonator.

- Surface Acoustic Wave (SAW) sensor: change in pressure → changes curvature of SAW substrate→changes SAW time-of-flight (Pohl and Seifert, IEEE Trans. Instr. Meas. (46):1031-1038, 1997), Figure 37.

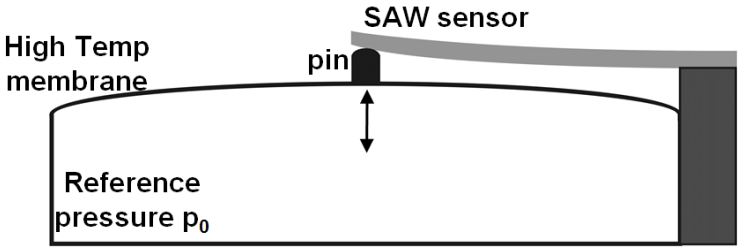

Figure 37. Surface Acoustic Wave Sensor.

- Bulk Acoustic Wave (BAW) Resonator: pressure → uniaxial stress to crystal via cylinder→changes BAW resonant frequency (Besson et al. IEEE Trans. Ultras. Ferroel. Freq. Cont. (40):584-591, 1993), Figure 38.

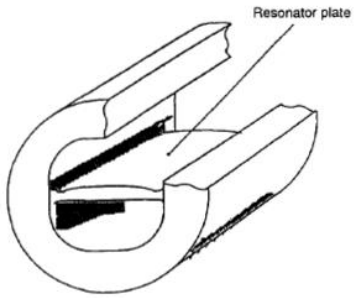

Figure 38. Bulk Acoustic Wave Resonator,from Besson et al.
IEEE Trans. Ultras. Ferroel. Freq. Cont. (40):584-591, 1993.

- Resonant Ultrasound Spectroscopy (RUS) of metal sphere.

  This sensing technique is based on the phenomenon of degenerate modes splitting under uni-axial stress. The Experimental setup consists of a function generator, a lock-in amplifier and an RUS rig consisting of two transducers facing each other, one acting as a transmitter and one as a receiver, see Figure 39. Different weights were used to obtain the uni-axial stress. An example is shown in Figure 40, for a 14.5 lbs load.

  The elastic moduli of the steel sphere used in this experiment were determined performing a fit of the experimental resonances, resulting in a bulk modulus of about 164 GPa, see Figure 41, in good agreement with literature values. However, we did not measure any noticeable change in the resonances as the uni-axial load was increased. This led us to the next approach, using a hollow metal sphere as the pressure sensing element.

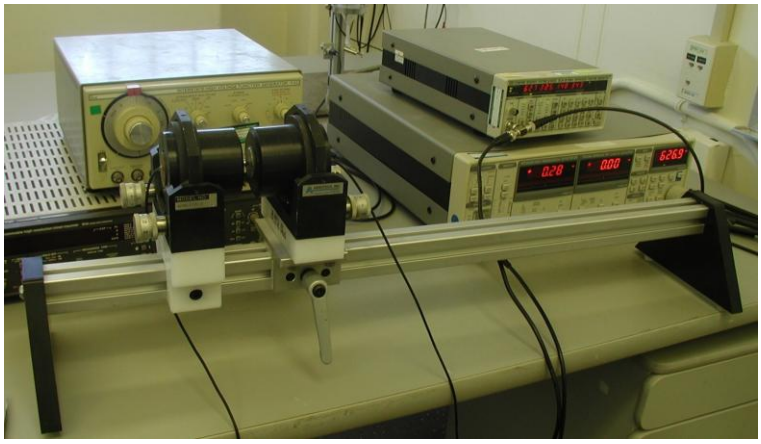

Figure 39. Experimental setup: RUS fixture, signal generator, frequency counter.

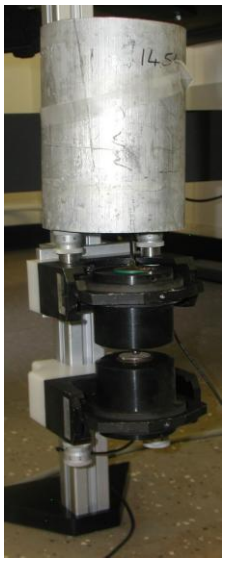

Figure 40. RUS fixture with 14.5 lb weight

```
 LANL Sphere code Ver. 6.0
   Steel sphere
free moduli are  c11, c44
using 14 order polynomials    mass=  2.0400 gm  rho= 7.813 gm/cc

  n     fex      fr      %err  wt  k  i    df/d(moduli)
   1 0.318885 0.319977   0.34 1.0  1  2  0.00  1.00
   2 0.320922 0.319977  -0.29 1.0  7  2  0.00  1.00
   3 0.321155 0.319977  -0.37 1.0  4  2  0.00  1.00
   4 0.000000 0.319977   0.00 0.0  6  2  0.00  1.00
   5 0.000000 0.319977   0.00 0.0  4  1  0.00  1.00
   6 0.337306 0.338410   0.33 1.0  5  1  0.03  0.97
   7 0.337703 0.338410   0.21 1.0  5  2  0.03  0.97
   8 0.339456 0.338410  -0.31 1.0  8  1  0.03  0.97
   9 0.000000 0.338410   0.00 0.0  2  1  0.03  0.97
  10 0.000000 0.338410   0.00 0.0  3  1  0.03  0.97
  11 0.448832 0.449444   0.14 1.0  7  3  0.35  0.65
  12 0.449292 0.449444   0.03 1.0  6  3  0.35  0.65
  13 0.000000 0.449444   0.00 0.0  1  3  0.35  0.65
  14 0.494647 0.494422  -0.05 1.0  3  3  0.00  1.00
  15 0.495097 0.494422  -0.14 1.0  5  3  0.00  1.00
  16 0.000000 0.494422   0.00 0.0  2  3  0.00  1.00
  17 0.000000 0.494422   0.00 0.0  3  2  0.00  1.00
  18 0.000000 0.494422   0.00 0.0  2  2  0.00  1.00
  19 0.000000 0.494422   0.00 0.0  8  3  0.00  1.00
  20 0.000000 0.494422   0.00 0.0  8  2  0.00  1.00
  21 0.501651 0.503299   0.33 1.0  1  5  0.06  0.94
  22 0.504217 0.503299  -0.18 1.0  6  5  0.06  0.94
  23 0.000000 0.503299   0.00 0.0  7  5  0.06  0.94
  24 0.000000 0.503299   0.00 0.0  7  4  0.06  0.94
  25 0.000000 0.503299   0.00 0.0  1  4  0.06  0.94
  26 0.000000 0.503299   0.00 0.0  4  3  0.06  0.94
  27 0.000000 0.503299   0.00 0.0  6  4  0.06  0.94
  28 0.626209 0.625780  -0.07 1.0  5  4  1.48 -0.48
  29 0.636605 0.637639   0.16 1.0  5  6  0.33  0.67
  30 0.637617 0.637639   0.00 1.0  5  5  0.33  0.67

Bulk Modulus=  1.64106

   c11    c22    c33    c23    c13    c12    c44    c55    c66
 2.6992 2.6992 2.6992 1.1120 1.1120 1.1120 0.7936 0.7936 0.7936

      d1       d2       d3
  0.79300  0.79300  0.79300

 loop# 2  rms error=  0.2305 %, changed by        -0.0001 %

 length of gradient vector=  0.008550  blamb=  0.000000

 eigenvalues    eigenvectors
    11.07577   1.00 0.01
   561.69179  -0.01 1.00

chisquare increased 2% by the following % changes in independent parameters
  0.02  0.00
  0.00  0.01
```

Figure 41. RUS fit of steel sphere, no load.

- Resonant Ultrasound Spectroscopy (RUS) of hollow metal spheres under uni-axial stress. Rigorous theoretical simulations were performed using COMSOL's acoustic module. An example is shown in Figure 42, where the first resonance mode of an Al hollow sphere at a pressure of 50 MPa is shown.

  A simplified RUS experimental drawing on an Al hollow sphere is shown in Figure 43. Two $LiNbO_3$ transducers positioned opposite to each other were used, one as a transmitter and another one as receiver.

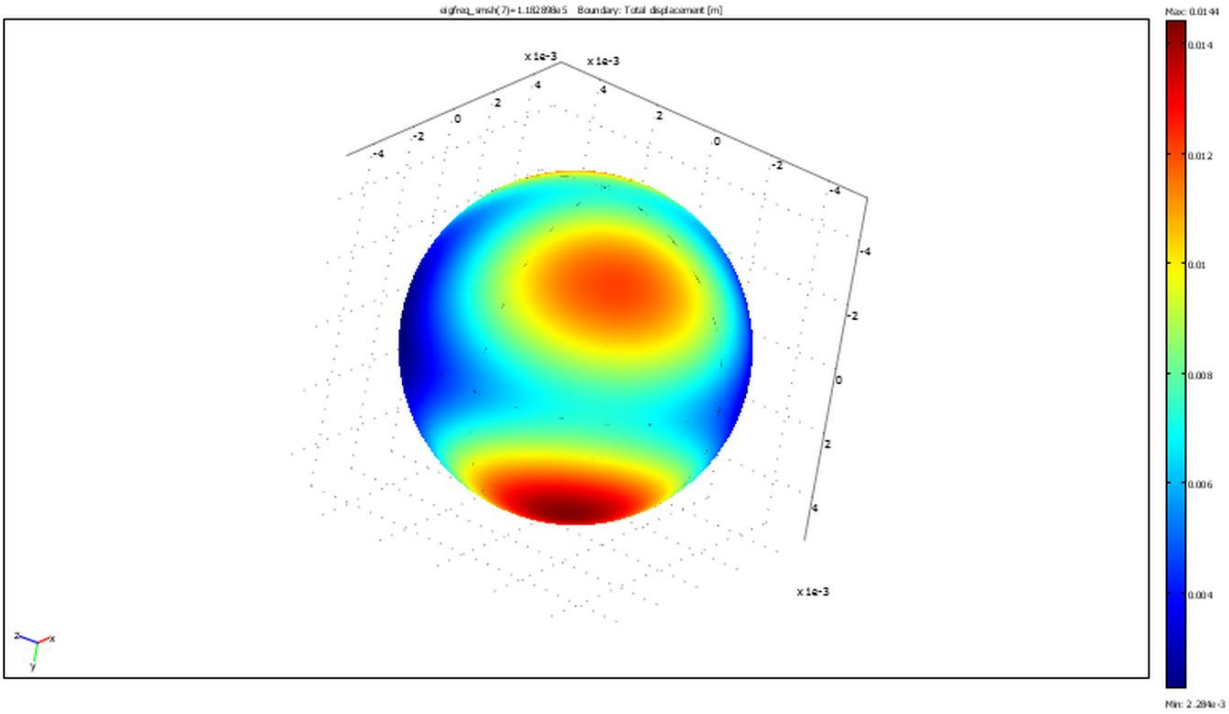

Figure 42. First resonance mode of an Al hollow sphere at 50 MPa pressure.

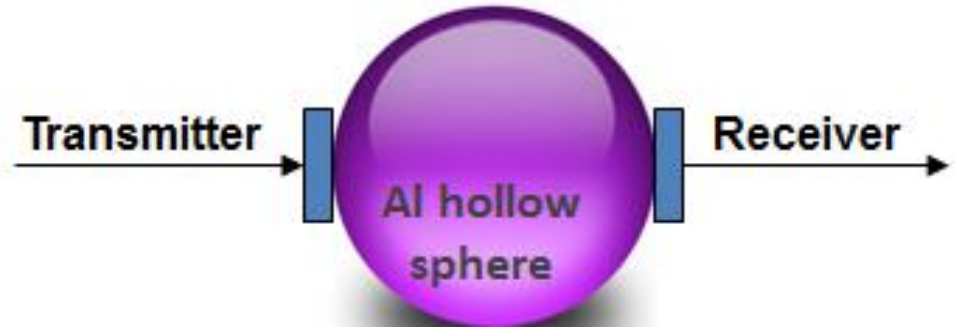

Figure 43. Drawing of a simplified Resonance Ultrasonic Spectroscopy experiment.

Hollow Aluminum spheres with diameters of 0.25, 0.375, 0.5 and 1 inch, respectively, were investigating under no load. The RUS spectra are shown in Figure 44. Characteristic resonances of Aluminum hollow spheres were investigated as load pressure was changed, see an example in Figure 45, for eight different loads. A zoom-in on the second degenerate mode (split frequency) is shown in Figure 46. Pressure can be determined relatively straightforward as illustrated in Figure 47, where two of the resonances of a degenerate mode do not change, while the third resonance is changing significantly with pressure.

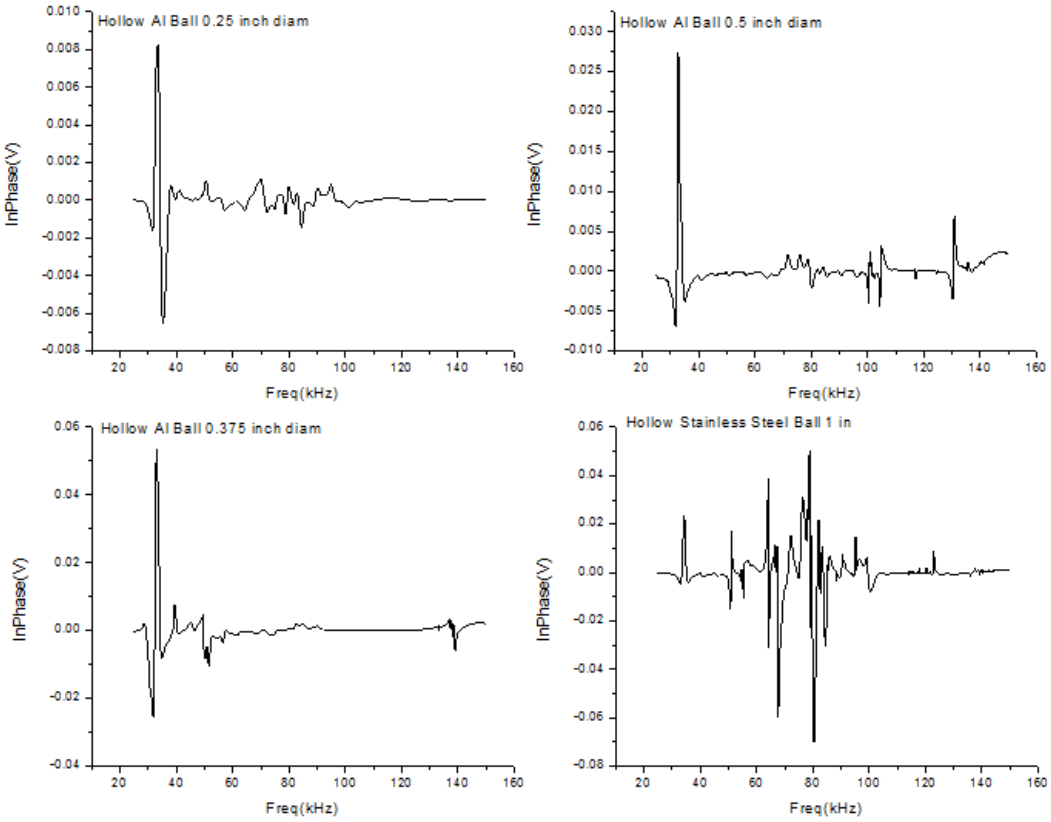

Figure 44. RUS spectra of hollow Al spheres with different diameters.

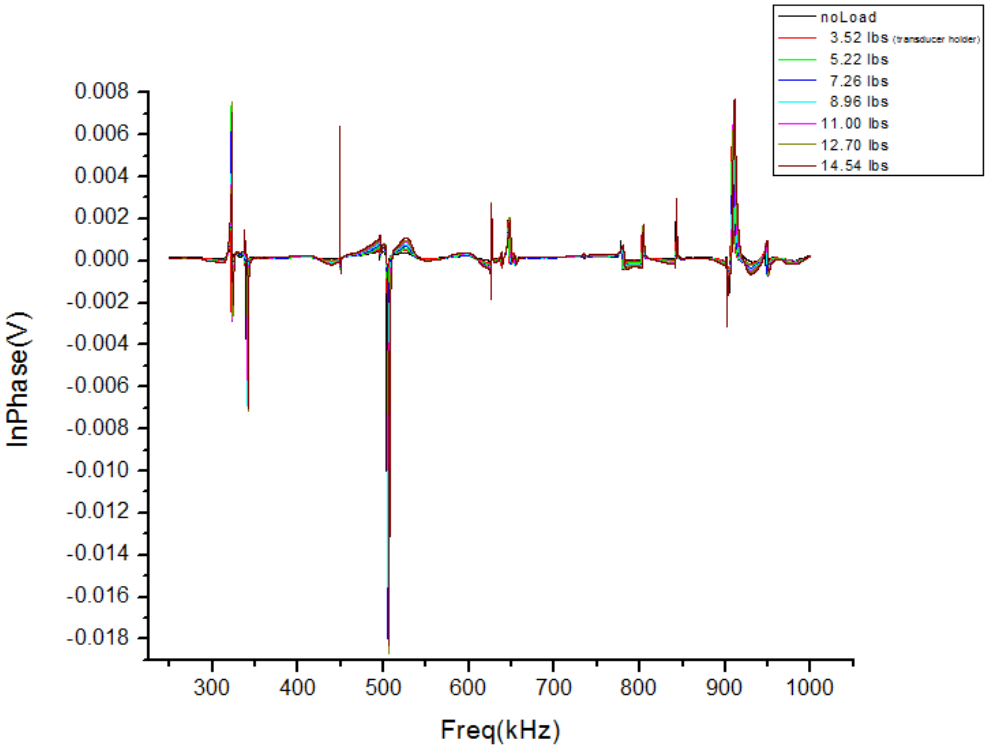

Figure 45. RUS spectrum of steel sphere vs. load

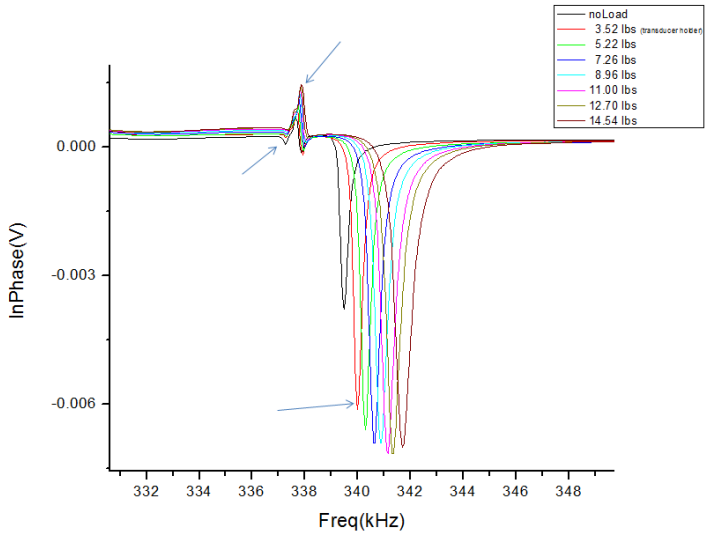

Figure 46. Second split peak frequency vs. load

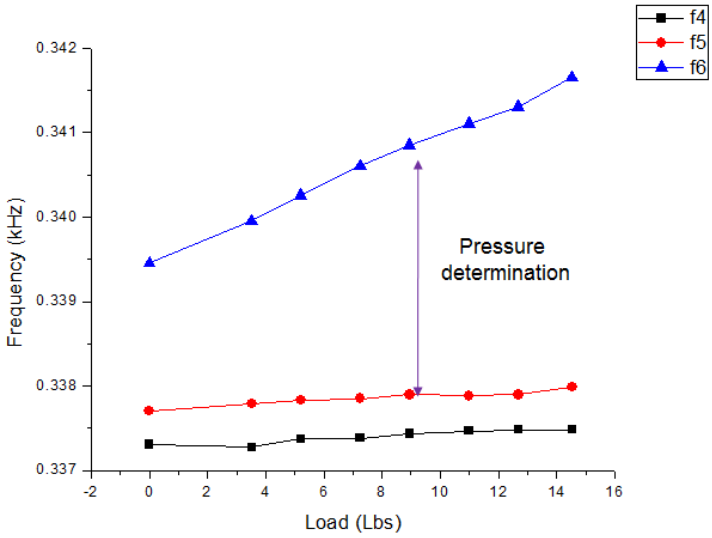

Figure 47. Degenerate mode with three split frequencies.

- Resonant Ultrasound Spectroscopy (RUS) of hollow metal spheres under uniform stress (hydrostatic pressure).

  Additional experiments were performed under hydrostatic pressure conditions. The main advantage of such a configuration is that the sensor depicted in Figure 43 can be placed downhole as-is, without any additional mechanical modifications. For uni-axial stress dependence the sensor requires conversion of hydrostatic pressure to uni-axial stress, which complicates significantly the sensor construction.

  Figure 48 shows the pressure dependence of a narrow set of resonances of an Al hollow sphere with hydrostatic pressure. Five different pressures were used, including room

pressure. Figure 49 shows the change of a specific resonance frequency with hydrostatic pressure, derived from the data presented in Figure 48. A good sensitivity of 1.6 ppm/psi was obtained.

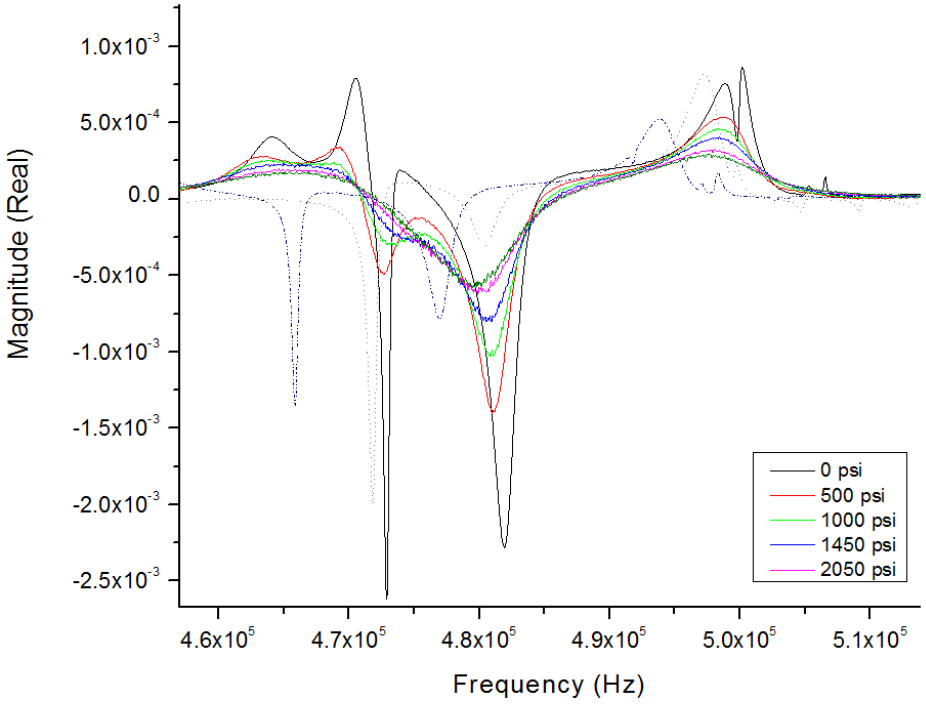

Figure 48. Al hollow sphere RUS spectra for different hydrostatic pressures.

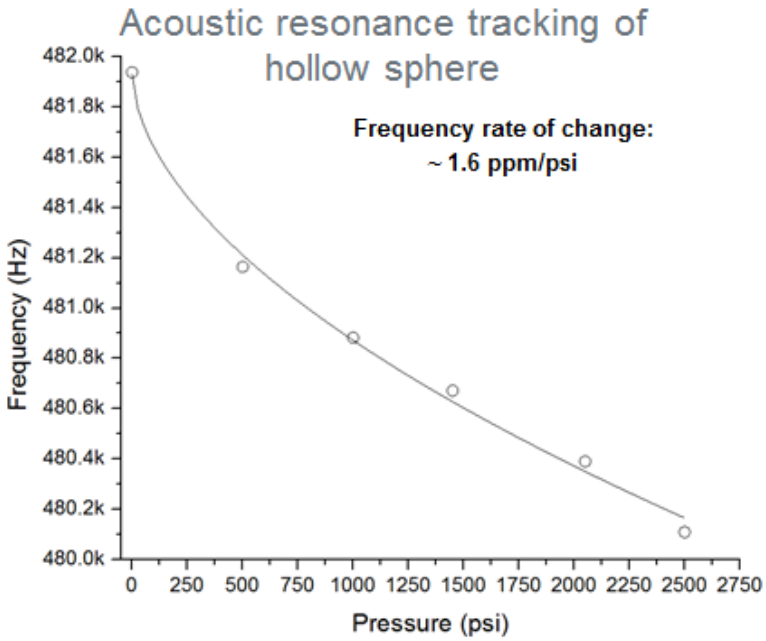

Figure 49. Frequency change with hydrostatic pressure.

Data sharing

- Type of data that is being generated from this project:

  - Conceptual development of a high temperature acoustic-based sensor for temperature, pressure and fluid properties determination

  - Generate numerical datasets related to brine physical properties at pressures and temperatures characteristic to EGSs
- Data can be uploaded to the "DOE Geothermal Data Repository" - currently under development by Boise State University. The DOE Geothermal Data Repository will be made public through the National Geothermal Data System, or retained in the DOE Geothermal Data Repository as business confidential, where applicable.

Challenges

- The most important challenge encountered was related to approval of the pressure system by the LANL pressure safety committee. This was a lengthy process. However, we anticipated this and it was taken into account at the proposal stage.
- Survivability of adhesives in high temperature liquid environment
  - Identified electrically insulating adhesive that withstands harsh test conditions.
  - Have acquired several promising candidates for electrically conductive adhesives.

Summary

- Identified and acquired sensor materials that can withstand adverse conditions characteristic of EGS.
- Identified and acquired equipment necessary for the multipurpose acoustic sensor development.
- Initiated work on theoretical modeling and algorithm development for data analysis.
- Initiated work on sensor geometry.
- Solved problems related to high uncertainty determination of temperature
  - The natural resonance of the 'pure compressional' mode of the transducer can't be used in temperature determination
  - However, lower vibrational modes can be used reliably.
- Performed sound speed measurements up to 270^0C and tested components up to 374^0C.
- Performed pressure and temperature determination.
- Performed fluid flow measurements at room temperature in an in-house flow-loop.

- Modeling and analysis software development progressing according to schedule.

The DOE Geothermal Technologies Program recently released two documents related to:

(1) High-priority technology needs into targeted technology focus areas. In the "Well Logging Tools" category, the target temperature for High Temperature Tools for year 2020, is 300°C. The maximum working temperature reached at the end of our project (Oct 2012) was 270°C. This can be further improved, subject to future funding.

Well Logging Tools

Advance logging tool technology as applied to geothermal

Technology Advancement	Technology Metrics			
	Metric Unit for Advancement	2011 Status	Target	When
Higher temperature tools	Temperature (°C)	150-200°C	300°C	2020
Slimhole geothermal logging tools	Diameter (in)	150-200°C	≤3"	2016

(2) Technology needs specific to EGS reservoir characterization, creation, and sustainability/operation. In the "High Temperature Logging and Imaging Tools" category, the set target for 2018 is ±10% precision for pressure, temperature and flow. It is to be noted that our lab measurements have already reached the targets set for 2018.

High Temperature Logging & Imaging Tools

Real-time mass "fluxometer" and integrated pressure/flow/temperature tool

Technology Advancement	Technology Metrics			
	Metric Unit for Advancement	2011 Status	Target	When
Mass "fluxometer"	Mass flux accuracy (l/s)	NEW	+/- 0.2 l/s	2015
Integrated Pressure/Flow/ Temp (PFT) Testing Tool	Precision (P, m/s, and T)	+/- 50%	+/- 10	2018

Awards/Recognition for Project or Researchers

Selected for one of the two technical presentations for the New Mexico Office of Recovery and Reinvestment leaders visit at LANL, Mar 30, 2010, represented by former NM governor Toney Anaya. Article featured in LANL today.

Publications and Presentations

1. 'Determination of the acoustic nonlinearity parameter in liquid water up to 250°C and 12 MPa', LA-UR-12-24843, B.T. Sturtevant, Dipen N. Sinha, Cristian Pantea, *IEEE Ultrasonics Symposium Proceeding, in press.*
2. 'An Acoustic Resonance Measurement Cell for Liquid Property Determinations up to 250°C', LA-UR-12-24498. Blake Sturtevant, Cristian Pantea, Dipen Sinha accepted in *Review of Scientific Instruments.*

3. 'Evaluation of the transmission line model for couplant layer corrections in pulse-echo measurements', LA-UR-12-23404. Blake Sturtevant, Cristian Pantea, Dipen Sinha, submitted to *IEEE Transactions on Ultrasonics, Ferroelectrics and Frequency Control.*
4. 'Acoustic Nonlinearity Measurements in FC-43 Fluorocarbon up to 100°C and 2000 PSI', B.T. Sturtevant, Dipen N. Sinha, Cristian Pantea, in preparation for submission to *J Appl Phys.*
5. 'Determination of the parameter of nonlinearity, B/A, in liquid water up to 250°C and 2000 PSI', B.T. Sturtevant, Dipen N. Sinha, Cristian Pantea, in preparation for submission to *IEEE Transactions on Ultrasonics, Ferroelectrics and Frequency Control.*

Presentations:

- B.T. Sturtevant, C. Pantea, D.N. Sinha, *Acoustic Nonlinearity Measurements in FC-43 Fluorocarbon up to 373 K and 13.8 MPa*, 164th Meeting of the Acoustical Society of America, Kansas City, Missouri, 22-26 Oct 2012.
- B.T. Sturtevant, C. Pantea, D.N. Sinha, *Determination of the acoustic nonlinearity parameter in liquid water up to 250°C and 12 MPa*, 2012 IEEE International Ultrasonics Symposium, Dresden, Germany, Oct 7-10, 2012.
- B.T. Sturtevant, C. Pantea, D.N. Sinha, *Coupling layer corrections in pulse echo time-of-flight measurements in solids revisited*, 161st Meeting of the Acoustical Society of America, Seattle, Washington, 23-27 May 2011.